

RUNNING HEAD:

WATER DEPTH CONTROL ON FLUVIO-MARINE SEDIMENT PARTITIONING

TITLE:

FLUVIO-MARINE SEDIMENT PARTITIONING AS A FUNCTION OF BASIN WATER DEPTH

JOCHEM. F. BIJKERK^{1,3}, JORIS T. EGGENHUISEN², IAN A. KANE⁴, NIELS MEIJER², COLIN N. WATERS³,
PAUL B. WIGNALL¹, WILLIAM D. MCCAFFREY¹

¹) School of Earth and Environment, University of Leeds, Leeds LS2 9JT, UK

²) Department of Earth Sciences, Utrecht University, PO Box 80021, 3508 TA Utrecht, The Netherlands

³) British Geological Survey, Environmental Science Centre Centre, Keyworth, Nottingham NG12 5GG, UK

⁴) Statoil ASA, Exploration, NO-1364 Oslo, Norway

Email: jochem.j.bijkerk@shell.com

KEYWORDS (5x):

Analogue modeling, sequence stratigraphy, longitudinal profiles, downstream fining, water depth

1. ABSTRACT

Progradational fluvio-deltaic systems tend towards but cannot reach equilibrium, a state in which the longitudinal profile does not change shape and all sediment is bypassed beyond the shoreline. They cannot reach equilibrium because progradation of the shoreline requires aggradation along the longitudinal profile. Therefore progradation provides a negative feedback, unless relative sea level falls at a sufficient rate to cause non-aggradational extension of the longitudinal profile. How closely fluvio-deltaic systems approach equilibrium is dependent on their progradation rate, which is controlled by water depth and downstream allogenic controls, and governs sediment partitioning between the fluvial, deltaic and marine domains. Here, six analogue models of coastal fluvio-deltaic systems and small prograding shelf margins are examined to better understand the effect of water depth, subsidence and relative sea-level variations upon longitudinal patterns of sediment partitioning and grain-size distribution that eventually determine large-scale stratigraphic architecture. Fluvio-deltaic systems prograding in relatively deep water environments are characterized by relatively low progradation rates compared to shallow water systems. This allows these deeper water systems to approach equilibrium more closely, enabling them to construct less concave and steeper longitudinal profiles that provide low accommodation to fluvial systems. Glacio-eustatic sea-level variations and subsidence modulate the effects of water depth on the longitudinal profile. Systems are closest to equilibrium during falling relative sea level and early lowstand, resulting in efficient sediment transport towards the shoreline at those times. Additionally, the strength of the response to relative sea-level fall differs dependent on water depth. In systems prograding into deep water, relative sea-level fall causes higher sediment bypass rates and generates significantly stronger erosion than in shallow water systems, which increases the probability of incised valley formation. Water depth in the receiving basin thus forms a first order control on the sediment partitioning along the longitudinal profile of fluvio-deltaic systems and the shelf clinoform style. It also forms a control on the availability of sand-grade sediment at the shoreline that can potentially be remobilized and redistributed into deeper marine environments. Key findings are subsequently applied to literature of selected shelf clinoform successions.

2. INTRODUCTION

Understanding sediment partitioning between the fluvial, deltaic and marine environments on geological time scales presents a major challenge in sedimentology and sequence stratigraphy (e.g. Bourget et al. 2013; Covault et al. 2011; Martinsen et al. 2010; Sømme et al. 2009). Sediment transport and its consequent depositional distribution along the longitudinal profile of alluvial rivers and delta systems can be understood through the concept of 'equilibrium' or 'grade' (Muto and Swenson 2005). Longitudinal profiles are generally concave up; their shape describing the decreasing gradient of alluvial river systems dependent on e.g. geological structure, geomorphology, water and sediment discharge parameters (e.g. Sinha and Parker 1996; Rice and Church 2001). When in equilibrium, all sediment is conveyed through the system without net erosion or deposition, implying that net sediment output is equal to sediment input, and thus that the shape of the longitudinal profile does not change (Fig. 1A).

Early morphological definitions of equilibrium and graded longitudinal profiles typically focus on small river segments over short time scales, and suggest that many rivers are in equilibrium (e.g. Mackin 1948; Schumm and Lichty 1965). Contrarily, Muto and Swenson (2005) suggest most fluvio-deltaic systems are in non-equilibrium because downstream deltaic deposition on geological time scales implies a lengthening of the longitudinal profile, which typically requires aggradation along this profile. Only during relative sea-level fall, non-aggradational extension of the fluvio-deltaic longitudinal profile is possible, which implies that equilibrium can be achieved (Muto and Swenson, 2005). We refer to this concept of equilibrium as system-scale equilibrium to distinguish it from older definitions.

50 System-scale equilibrium of fluvio-deltaic systems in sedimentary basins is typically in the
51 order of 10^5 to 10^6 y (Paola et al. 1992a), and is approached asymptotically (Postma et al. 2008).
52 Analogue and numerical modeling shows that fluvio-deltaic systems that are far removed from
53 equilibrium approach this state rapidly by using a large percentage of the sediment load for
54 aggradation of the fluvial system (Postma et al. 2008). Conversely, systems that are close to
55 equilibrium conditions develop towards this state more slowly using a small percentage of the
56 available sediment load while most sediment is bypassed beyond the shoreline. How closely systems
57 approaches system-scale equilibrium thus controls the sediment volume used for aggradation along
58 the longitudinal profile and the sediment volume available for progradation of the shoreline. This
59 represents a negative feedback mechanism in which the magnitude of the departure from system-
60 scale equilibrium (Voller and Paola 2010) determines fluvio-marine sediment partitioning, thereby
61 setting the progradation rate, which determines the departure from system-scale equilibrium (Fig.
62 1B).

63 Water depth forms a primary control on progradation rate and might thus influence
64 aggradation rates along the longitudinal profile via the above described feedback mechanism.
65 Additionally, relative sea-level variations can significantly affect shoreline migration rates as well as
66 the position of the equilibrium profile relative to the actual longitudinal profile of coastal fluvio-
67 deltaic systems (Wheeler 1964). This is used in sequence-stratigraphic models to define whether a
68 system is in net erosional or depositional state (e.g. Catuneanu et al. 2009; Posamentier and Vail
69 1988; Shanley and McCabe 1994). If relative sea level falls at such rate that the coastal trajectory is
70 exactly an extension of the equilibrium profile, progradation is not associated with aggradation
71 along the longitudinal profile, which therefore can reach equilibrium (Helland-Hansen and Hampson
72 2009; Muto and Swenson 2005). More severe relative sea-level fall, such as associated with
73 erosional unconformities and incised valley systems, can lower the equilibrium profile to below the
74 coastal plain segment of the longitudinal profile resulting in net erosion and efficient sediment
75 transport from the hinterland to the river mouth. Conversely, during relative sea-level rise the
76 conceptual equilibrium profile is raised, resulting in the creation of accommodation on the coastal
77 plain. Subsequently, this results in reduced sediment transport to the shoreline and in thick coastal
78 plain deposits.

79 In an upstream direction, the influence of relative sea-level variations is gradually reduced
80 while controls such as water discharge, sediment supply, and tectonic regime increasingly influence
81 sediment transport and the grade of systems (e.g. Catuneanu et al. 2009; Holbrook and
82 Bhattacharya 2012; Posamentier and James 1993). Tectonic subsidence or uplift strongly determines
83 long term accommodation trends along the longitudinal profile (Miall 2013). Water and sediment
84 discharge variations can alter the steepness of the equilibrium profile over relatively short time
85 scales, resulting in alternating periods of aggradation and downcutting of fluvial systems that
86 continuously develop towards new equilibrium profiles (Bijkerk et al. 2013; Holbrook et al. 2006;
87 Simpson and Castelltort 2012). Fluvio-deltaic systems thus respond to the combined effect of
88 upstream and downstream allogenic forcing mechanisms (e.g. Hampson et al. 2013), as well as
89 inherent processes such as progradation, and tend towards a system-scale equilibrium state through
90 continuous adjustments of the longitudinal profile. These adjustments shift sediment partitioning
91 between the fluvial, deltaic and marine environments of a sedimentary system and therefore
92 determine the large-scale stratigraphic architecture.

93 The purpose of this contribution is to quantify how downstream external controls such as
94 water depth in the receiving basin, eustatic sea-level variations and subsidence rates affect the
95 ability of a prograding fluvio-deltaic system to approach system-scale equilibrium, and how this
96 affects sediment volume partitioning in fluvio-deltaic systems. This concept is examined through
97 landscape models of fluvio-deltaic systems. We consider these models analogous to the coastal
98 segment of fluvio-deltaic systems that supply sediment to shelf clinoforms into basins of up to a few
99 100's m depth (Helland-Hansen et al. 2012), such as frequently found in foreland or rift basins as the

100 Carboniferous Central Pennine Basin of northern England (Bijkerk 2014; Martinsen et al. 1995) or the
101 Eocene Central Basin of Spitsbergen (e.g. Plink-Björklund and Steel 2006). Additional two-
102 dimensional models are generated to examine the effect of progradation on the development of the
103 longitudinal profile in terms of downstream fining. Subsequently, literature case studies of ancient
104 small shelf clinoform systems are used to validate our findings.

105 3. METHODS

106 3.1 Experimental facility

107 The results of four analogue models are described. The experimental setup consisted of a
108 dual-basin configuration and allowed generation of two scenarios simultaneously: Model 1 (M1) and
109 Model 2 (M2) (Fig. 2). Both models had a 1.6 m wide rectangular duct serving as a fluvial zone that
110 was connected to a subsiding basin that deepened away from the shoreline with discrete shallow,
111 intermediate and deep zones. Sediment and water entered the experiment diffusely through a
112 pebble basket along the width of the fluvial duct. This setup allows the system to aggrade or degrade
113 freely and does not enforce an upstream control on the elevation at which sand and water enter the
114 experiment. Before an experiment, the longitudinal profile of each model was set to a downstream
115 gradient of 0.01. The models had different subsidence scenarios, but reached the same basin shape
116 and depth at the end of the experiments (Fig. 3). Subsidence is generated with vertical adjustment of
117 hexagonal blocks underneath the experimental set-up. Rows of these blocks are connected by
118 overlying boards to generate smooth, rather than serrated, subsidence zone boundaries (Fig. 2). An
119 adjustable overflow controls the basinal water level during these experiments. All models are
120 executed with fine quartz sand of a narrow grain-size distribution ($D_{10} = 146 \mu\text{m}$, $D_{50} = 217 \mu\text{m}$, and
121 $D_{90} = 310 \mu\text{m}$).

122 In Experiment 1 - Model 1 (E1_M1), the effects of water depth are tested. Before starting
123 this experiment, its basin was subsided to its final configuration. Therefore, this system experiences
124 only a spatial increase in water depth as it progressively enters the shallow, intermediate and deep
125 zones of the experimental basin (Fig. 2; Fig. 3A). In Experiment 1 - Model 2 (E1_M2) the joint effects
126 of subsidence and water depth are tested (Fig. 3A, B). During the first half of the experiment, the
127 fluvio-deltaic system progrades over a non-subsiding substrate in shallow water, whilst during the
128 second half the basinal area subsides at a rate of 2.5 mm h^{-1} . This results in subsidence-controlled
129 accommodation on the delta plain, and both temporally and spatially increasing water depths (Fig. 2;
130 Fig. 3B). In both E1_M1 and E1_M2 water discharge and sediment input were constant at $1 \text{ m}^3\text{h}^{-1}$
131 and $0.004 \text{ m}^3\text{h}^{-1}$, respectively.

132 In Experiment 2, basinal water-level variations are also included to mimic eustatic sea-level
133 variations, with different subsidence and discharge regimes for Model 1 (E2_M1) and Model 2
134 (E2_M2) (Fig. 3C, D; Table 1). Both models are affected by three asymmetric water-level cycles of 24
135 h period and variable amplitude. Cycle 1 starts with a 40 mm fall, followed by a 30 mm rise. Cycle 2
136 has a 20 mm fall and rise, and cycle 3 has a 30 mm fall, followed by a 40 mm rise, returning the
137 water level to the initial level (Fig. 3C, D). In E2_M1, the subsidence rate is continuous throughout
138 the experiment, resulting in the creation of accommodation on the delta plain, and progradation
139 into increasingly deeper water (Fig. 3C). Upstream, water discharge and sediment input were
140 constant at $1.5 \text{ m}^3\text{h}^{-1}$ and $0.004 \text{ m}^3\text{h}^{-1}$ (Table 1). Water discharge is at a higher rate than in other
141 models and theoretically leads to a faster equilibrium time and lower equilibrium gradient (e.g.
142 Postma et al., 2008). In E2_M2, the entire basinal area is lowered 15 mm to accommodate water-
143 level lowstand 1 (at 16 h) before the experiment starts. Subsidence at different rates for the shallow,
144 intermediate and deep zones starts after 24 h (Fig. 3D). In E2_M2 values are $1 \text{ m}^3\text{h}^{-1}$ for water
145 discharge and $0.004 \text{ m}^3\text{h}^{-1}$ for sediment discharge, which is equal to the values in Experiment 1
146 (Table 1).

147

148

3.2 Experimental procedure

149

150

151

152

The fluvio-deltaic systems were allowed to prograde during a start-up period prior to the actual experiment, so that experiments commenced with a natural, self-adjusted fluvial profile that reached the basin margin at 0 h (Fig. 2). Basinal water level during this period was 0 mm. Time-lapse photographs were taken at 3 minute intervals to record the morphology of the fluvio-deltaic system.

153

154

155

156

157

The 96 h duration of E1_M1 and E1_M2 was subdivided into 12 intervals of 8 h (Table 1). Subsidence was applied to E1_M2 between these 12 intervals while the experiment was paused. Digital elevation models (DEMs) were measured with a laser scanner before and after subsidence to accurately constrain sediment budgets. The 72 h duration of E2_M1 and E2_M2 was similarly subdivided in 8 h intervals. Water level was adjusted at 20 min intervals.

158

159

3.3 Scaling

160

161

162

163

164

165

166

In the scaling of analogue models emphasis is placed on the stratigraphic similarity to real-world sedimentary systems, interpreting the large-scale stratigraphic patterns of such models as controlled miniature versions of such systems. In recent years, this type of experiment is increasingly recognized as a powerful tool in understanding the stratigraphic behavior of sedimentary systems in both space and time (e.g. Paola et al. 2009). The small size of these models allows for rapid simulation of the stratigraphic architecture of real world systems but does not incorporate properly scaled sedimentary processes and resultant facies.

167

168

169

170

171

172

173

174

175

176

177

The scaling relation between real-world landscapes and analogue experiments is based on characteristic length and time scales. Length scales (e.g. the length of the depositional segment of a river) are easily established while time scales associated with stratigraphic development over such length scales are approached by non-linear diffusion equations (Paola et al. 1992a; Postma et al. 2008). Using an analogue scaling approach, landscape experiments can be set up to mimic the stratigraphic response of real-world systems to allogenic and autogenic controls. Landscape models have successfully reproduced stratal patterns that are commonly recognized in sequence-stratigraphic models such as incised valleys, sequence boundaries, maximum flooding surfaces, and system tracts (e.g. Koss et al. 1994; Martin et al. 2011; van Heijst et al. 2002; van Heijst and Postma 2001), while being able to determine the relative importance of controls (e.g. Kim and Paola 2007; Kim et al. 2006; Muto and Swenson 2006).

178

179

180

181

182

183

184

185

186

187

The style and record of responses of natural systems on forcing mechanisms depends on the ratio between time scales of forcing (T_{for}) and reactive time scales inherent to the system. For stratigraphic architecture, this reactive time scale has been termed the equilibrium time (T_{eq}) (Paola et al. 1992a). The ratio of T_{for}/T_{eq} has proven to be effective for the simulation of stratigraphic response to various rates of relative sea-level variations (Bijkerk et al. 2013; Paola et al. 2009; Strong and Paola 2008; van Heijst and Postma 2001). Slow processes ($T_{for} \gg T_{eq}$) are unable driving a system away from equilibrium conditions because the system has sufficient time to adapt to new boundary conditions. Fast processes ($T_{for} \ll T_{eq}$) on the other hand can strongly affect the grade of a fluvio-deltaic system because it is incapable of adapting at sufficiently fast rates to keep up with the forcing mechanism.

188

189

190

191

192

193

194

195

For well-constrained systems such as modern river systems and analogue models, diffusion equations can be used to describe sediment transport. The squared length of a fluvial system, divided by its diffusivity provides an estimate of the equilibrium time (Paola et al. 1992). Diffusivity is a function that is strongly dependent on water discharge per unit width and stream type. For braided systems it is approximated by a tenth of the width-averaged water discharge (Paola et al. 1992a). In E1_M1, E1_M2 and E2_M2 this results in an estimated equilibrium time of ~100 h at the start of the experiment. For E2_M1, the higher water discharge results in a higher diffusivity and thus in a shorter equilibrium time of ~72 h. The 24 h water-level cycles in Experiment 2 thus

196 approximate a quarter (where $T_{eq} \sim 100$ h) or third (where $T_{eq} \sim 72$ h) of the estimated equilibrium
197 time. Such ratios fall within the same range as many modern fluvial systems that are affected by 100
198 kyr eustatic sea-level cyclicity and have equilibrium times in the order of 100 – 1000 kyr (cf.
199 Castellort and Van Den Driessche 2003). The cyclic variations in the water level of Experiment 2 thus
200 mimic high frequency sea-level variation relative to the equilibrium time of the fluvio-deltaic system
201 that are best compared to the high frequency, high amplitude glacio-eustatic sea-level variations.
202 Therefore, the used water-level curve is asymmetric with the duration of water-level fall twice as
203 long as water-level rise as to mimic 100 kyr glacio-eustatic sea-level variations (e.g. Lisiecki and
204 Raymo 2005).

205 The 20 – 40 mm water-level variations are representative of glacio-eustatic sea-level
206 variations that typically range from 50 – 100 m. Therefore the 80 –120 mm water depths in the
207 intermediate and deep zones (Fig. 2) are analogous to water depths of up to several 100's meters.
208 This implies that we are mimicking depositional systems that are typically defined as small shelf
209 clinofolds (e.g. Helland-Hansen et al. 2012; Carvajal and Steel 2006; Plink- Björklund and Steel,
210 2007; Steel et al. 2007). Because we mimic progradation of a small shelf clinofold, we have opted
211 for a fluvial line-source instead of a point source, as the latter would result in the construction of a
212 fan delta geometry (e.g. Heijst and Postma, 2001). The subsidence patterns represent variable
213 tectonic scenarios in which subsidence increases away from the basin margin, and allow us to study
214 their effect on the development of the longitudinal profile.

215 *3.4 Dataset*

216 Analyses are based on DEMs and supported by time-lapse images. DEM analyses are focused
217 on the shape of the longitudinal profile, and the percentage of sediment input that is transported
218 past the shoreline during successive 8 h intervals.

219 The shape of the experimental longitudinal profiles is typically concave up. Laterally, both
220 the concavity and elevation of the longitudinal profile vary for each DEM (Fig. 4). To express the
221 shape of the longitudinal profile a 'fill percentage' and a 'slope percentage' are calculated to express
222 the concavity and the overall changes in gradient of the longitudinal profile, respectively (Fig. 4A).
223 This method was chosen because a curve-fitting approach produced insufficiently accurate results
224 and was therefore unsuitable to pick up minor variations in the shape of the longitudinal profile (e.g.
225 Ohmori 1991; Rice and Church 2001; Snow and Slingerland 1987).

226 Along the width of the models, a series of imaginary right-angled triangles can be drawn
227 between the top of the longitudinal profile, the roll-over point, and an upstream point at the same
228 elevation as the roll-over point DEM (Fig. 4A). The 'fill percentage' is defined as the volume
229 percentage of these triangles that is below the actual sediment surface. A horizontal plane would
230 represent 0% fill while a linear sloping profile would represent a 100% fill of the longitudinal profile.
231 Intermediate values provide a volumetric measure of the concavity of the longitudinal profile
232 without focusing on the precise shape of such profile (Fig. 4A).

233 In a similar way, the longitudinal profile can be expressed as a 'slope percentage', which can
234 indicate temporal changes in the gradient of the longitudinal profile (Fig. 4A). This is here defined as
235 the ratio between the sediment volume below the sediment surface and the volume below the
236 estimated system-scale equilibrium gradient. In this case, a horizontal plane would represent 0%
237 value while a 100% value would represent system-scale equilibrium conditions. The estimated
238 system-scale equilibrium gradient is based on the gradient of the longitudinal profile of E2_M1 at 16
239 h, when the system achieved a near-linear, steep slope, and 100% sediment bypass over a period of
240 8 h, implying conditions at, or close to system-scale equilibrium.

241 The water discharge and the water to sediment discharge ratio in E2_M1 are higher than in
242 the other experiments (Table 1) resulting in more efficient sediment transport at lower gradients.
243 This also implies that the model has a lower equilibrium gradient compared to the other models

244 (e.g. Postma et al. 2008). Because the estimation for the system-scale equilibrium gradient was
245 derived from experiment E2_M1 at 16 h , a conversion is required to estimate the system-scale
246 equilibrium gradient in the other models: E1_M1, E1_M2, and E2_M2. This conversion is based on
247 the difference in longitudinal gradient between E2_M1 and E2_M2 at 0 h. At this time only water
248 discharge differed while downstream parameters were equal. The 1.5 times higher water discharge
249 in E2_M1 resulted in a 1.2 times shallower gradient, relative to E2_M2. Consequently, the system-
250 scale equilibrium gradient in E1_M1, E1_M2, and E2_M2 is assumed at a 1.2 times steeper gradient
251 than in E2_M1. This conversion is basic but yields results consistent with the expectations that the
252 'slope percentage of the longitudinal profile' in the other models does not reach as high as in
253 E2_M1. Still, comparison of the 'slope percentage' of E2_M1 to other models depends on the
254 validity of the above assumption.

255 Additionally, DEMs are used to calculate the ratio between sediment volume used for
256 progradation and the total sediment volume, quantifying the efficiency of sediment transport to
257 beyond the shoreline (Fig. 4B).

258

259

3.5 Grain-size experiments

260 Besides the four landscape experiments described above, Scenario 1 and Scenario 2 were
261 run in a 0.48 m wide, 12 m long rectangular recirculation flume (Fig. 5). These models examine
262 downstream sediment fining as a function of the fluvio-deltaic system ability to approach system-
263 scale equilibrium. Quartz sand with a bimodal grain-size distribution was used with peaks at 216 μm
264 and 420 μm ($D_{50} = 285 \mu\text{m}$). The coarse-grained tail with a diameter of $>1 \text{ mm}$ (7% by weight) was
265 used to assess downstream fining.

266 Water was recirculated to the upstream side of the flume, resulting in a constant water
267 discharge of $5.5 \text{ m}^3\text{h}^{-1}$ (Table 1; Fig. 5). The large width of the upstream weir functions to accelerate
268 the slow-moving, large water column such that a thin water film enters the experiment at a constant
269 velocity (Fig. 5). On top of this upstream weir, dry sediment was added through an overhead
270 sediment feeder at a rate of $0.007 \text{ m}^3\text{h}^{-1}$ (Table 1; Fig. 5).

271 Instead of starting with a natural, self-adjusted fluvial profile such as the previously
272 described experiments, these experiments started as a 4 m horizontal plane. In this experiment, data
273 recording starts while the system aggrades to its natural gradient. In Scenario 1, a downstream weir
274 prevents progradation, allowing aggradation from horizontal plane up to the system-scale
275 equilibrium gradient (cf. Muto and Swenson 2005; Postma et al. 2008). In Scenario 2, downstream of
276 the horizontal plane, a basin of 3 cm water depth is present that allows shallow water progradation.

277 Both Scenario 1 and 2 ran for 8 h (Table 1; Fig. 5). At half hour intervals, five point-
278 measurements along the width of the flume at 0.25 m intervals were made to obtain a width-
279 averaged longitudinal profile (Fig. 5B). In both experiments, grain-size samples of the final
280 longitudinal profile were taken at 0.5 m intervals after the experiment finished. Additional grain-size
281 samples were taken behind the downstream weir of Scenario 1.

282 Water discharge was chosen such that average water depth on the fluvial topset was
283 sufficient to prevent preferential transport of coarse grains (cf. Vollmer and Kleinhans 2007). This
284 resulted in the formation of current ripples but enabled assessment of the relation between
285 downstream fining and longitudinal profile development. The approximate equilibrium time at the
286 start of these models is $\sim 14 \text{ h}$, based on diffusion equations controlled by the length and width-
287 averaged water-discharge of this system (Paola et al. 1992).

288

289

4. RESULTS

290

4.1 Experiment 1 - Basin 1 (E1_M1)

291 E1_M1 represents a pre-formed basin with constant water level and results in progradation
292 of a shelf clinoform system into a spatially deepening basin (Fig. 6A – C; Fig. 8A, B). The fill
293 percentage of the longitudinal profile increases from 91% to ~96% from 1 – 56 h and subsequently
294 decreases to 94% (Fig. 6G), indicating that the concavity initially decreases before increasing again
295 (Fig. 4A). The slope percentage of the longitudinal profile starts at 76% and increases to 92% from 1
296 – 56 h indicating that the longitudinal gradient steepens, after which it remains constant (Fig. 4A;
297 Fig. 6H). These trends correlate well with the sediment bypass pattern, which starts at ~24% of the
298 sediment input volume and increases towards a maximum of 50% from 56 – 64 h, implying that
299 increasing sediment volume is transported to beyond the shoreline. Subsequently, it decreases to
300 ~43% (Fig. 4B; Fig. 6F).

301 Over the duration of the experiment, the average clinoform height, measured along the
302 strike of the clinoform, gradually increases from 25 – 96 mm during the experiment and correlates
303 with the sediment bypass percentage and the fill and slope percentages (Fig. 6C, F – H). The
304 progradation rate decreases from 14 – 9 mm h⁻¹ (Fig. 6E) and results in a gradual increase in the size
305 of the longitudinal profile from 2.6 – 6.1 m² (Fig. 6D).

306

307 *4.2 Experiment 1 - Basin 2 (E1_M2)*

308 E1_M2 initially forms in a shallow ramp-style basin with constant water level that from 48 h
309 onwards subsides at a rate of 2.5 mm h⁻¹ (Fig. 7A, B). Shallow water conditions allow for rapid
310 progradation during the first half of the experiment. During the second half, tectonic subsidence
311 results in accommodation on the topset and in a deepening of the basin, which reduces the
312 progradation rate (Fig. 7C – E; Fig. 8 C, D). At the start of the experiment, sediment bypass is 5% of
313 the sediment input and increases to ~16% at 40 – 48 h (Fig. 7F). The initiation of subsidence reduces
314 sediment bypass to 8% (Fig. 7F, 48 – 56 h) after which it steadily increases to 24% at the end of the
315 experiment (Fig. 7F, 88 – 96 h). The fill percentage of the longitudinal profile starts at 86% and
316 increases rapidly towards 92% at 64 h (i.e. becomes less concave; Fig. 4A) at which point it becomes
317 approximately constant (Fig. 7G). The slope percentage of E1_M2 initially remains low at 74% (i.e.
318 progrades at a low gradient) and gradually increases to 87% after the initiation of subsidence,
319 implying that the gradient becomes steeper (Fig. 7E, H; Fig 4A).

320 Sediment bypass is low in the rapidly prograding system and coincides with a strongly
321 concave, low-gradient longitudinal profile (Fig. 7E – H, 0 – 48 h). After 48 h, the basin subsides
322 rapidly and a significant sediment volume is captured for topset aggradation, decreasing the
323 sediment bypass rate (Fig. 7E – H, 48 – 72h; Fig. 8C, D). Notably, towards the end of the experiment
324 this sediment bypass rate increases to its highest levels (Fig. 7C, E, F, 72 – 96 h). This coincides with
325 slow deep-water progradation and corresponds to an increasing fill and slope percentage of the
326 longitudinal profile (Fig. 7E – H), indicating a decreased concavity and an increased longitudinal
327 gradient compared to earlier parts of this experiment (Fig. 4A).

328

329 *4.3 Experiment 2 - Basin 1 (E2_M1)*

330 Throughout this experiment, subsidence is continuous and the water level in the receiving
331 basin mimics three glacio-eustatic cycles of constant frequency and variable amplitude (Fig. 9A). This
332 results in three regression – transgression cycles (Fig. 8E, F) that are reflected in the cyclicity of the
333 measured parameters (Fig. 9C – H).

334 The style of deposition and erosion changes significantly during a mimicked sea-level cycle
335 and varies between cycles as well (Fig. 11; Fig. 12). During normal regression, the entire fluvio-
336 deltaic topset is frequently active (Fig. 11A). During forced regression, two modes occur: small parts
337 of the topset become inactive, generating short-lived interfluves in cycle 1, 2 and the start of 3 (Fig.

338 11B). During relative sea-level fall 3, an incised valley forms that focuses much of the water and
339 sediment discharge along a narrow section of the delta topset, generating long-lived interfluves (Fig.
340 11C). This leads to significant progradation focused at the deep water segment of the basin, after
341 which the valley mouth shifts towards the shallower segment at a later stage (Fig. 11D). During
342 transgression, small lobes step back onto the lowstand shelf while in an upstream direction
343 discharge is still focused in the incised valley (Fig. 11E).

344 The fill and slope percentages, proxies for concavity and gradient of the longitudinal profile
345 (Fig. 4A; Fig. 9G, H), as well as sediment bypass beyond the shoreline show close correspondence to
346 the relative sea-level variations (Fig. 9B, F). The highest bypass rates are observed during late sea-
347 level fall and lowstand and coincide with increasing fill and slope percentages of the longitudinal
348 profile (i.e. longitudinal profiles become less concave and steeper; Fig. 9F – H, 8 – 16 h, 32 – 40 h, 56
349 – 64 h). Low sediment bypass occurs during the sea-level rise and coincides with a decreasing fill and
350 slope percentage of the longitudinal profile (i.e. longitudinal profiles become more concave and less
351 steep; Fig. 9F – H, 16 – 24 h, 40 – 48 h, 64 – 72 h). Intermediate rates for sediment bypass, fill and
352 slope percentage of the longitudinal profile occur during sea-level highstand and early sea-level fall
353 (Fig. 9F – H, 0 – 8 h, 24 – 32 h, 48 – 56 h).

354 During late relative sea-level fall in cycles 1, 2, and 3 the sediment bypass rate is 102, 63 and
355 126% of the sediment input, respectively (Fig. 9F). Sea-level fall 3 is smaller than sea-level fall 1 (30
356 vs. 40 mm) but results in incised valley formation and significantly higher sediment bypass (Fig. 9F).
357 Valley incision coincides with an increased water depth in the receiving basin and an increased fill
358 percentage of the longitudinal profile indicating a decreased concavity (cf. Fig. 9C, G, 8 – 16 h & 56 –
359 64 h). Interestingly, it also coincides with a reduced slope percentage relative to the first sea-level
360 fall (cf. Fig. 9H, 16 h & 64 h), indicating that erosion within the incised valley occurs at a lower
361 gradient than during sea-level fall 1.

362 Erosion-deposition maps also show that during relative sea-level fall 3 significantly more
363 erosion occurs on the delta topset than during relative sea-level fall 1 (Fig. 12A, C). In the case of
364 relative sea-level fall 3, erosion migrates upstream and results in significant erosion that persists
365 until the end of the subsequent relative sea-level rise (Fig. 12D).

366

367 *4.4 Experiment 2 - Basin 2 (E2_M2)*

368 The input parameters of E2_M2 differ from E2_M1 in two ways. Firstly, water discharge is 1
369 m^3h^{-1} instead of $1.5 \text{m}^3\text{h}^{-1}$ (Table 1). Secondly, the system progrades on a shallow, non-subsiding
370 ramp during sea-level fall 1, resulting in the very shallow water conditions at lowstand 1 (Fig. 10A, B,
371 8 – 16 h).

372 Sediment bypass shows a similar response to relative sea-level variation as in E2_M1 but
373 bypasses a smaller percentage of the sediment beyond the shoreline. The fill percentage of the
374 longitudinal profiles is lower, indicating that these profiles are more concave (cf. Fig. 9G & 10G). A
375 second difference is that the fill and slope percentages of the longitudinal profile decrease during
376 sea-level fall to lowstand at 16 h, whereas in E2_M1, these values increase (cf. Fig. 10G, H & Fig. 9G,
377 H, 16 h). This difference coincides with very high progradation rates and shallow water depth of <
378 5mm in the basin (Fig. 10C, E, 8 – 16 h).

379

380

381 *4.5 Grain-size experiments*

382 Scenarios 1 and 2 indicate that the development of the longitudinal profile and the grain-size
383 distribution along this profile are dependent on the progradation rate (Fig. 13). In Scenario 1 a weir
384 obstructed progradation, which resulted in the gradual development of an increasingly steeper

385 longitudinal profile (Fig. 13A). Towards the end of the experiment successive profiles overlap along a
386 steep and nearly linear longitudinal profile, indicating that the profile did not aggrade significantly
387 after 5.5 h (Fig. 13A). Grain-size data collected below the downstream weir (Fig. 5) indicate that after
388 4.5 h coarse-grained fraction bypassed the weir approximately at the same ratio as the input ratio,
389 indicating that downstream fining was no longer efficient (Fig. 13C). This is further supported by
390 samples along the final longitudinal profile that do not indicate a downstream fining trend (Fig. 13B).

391 In Scenario 2, the fluvio-deltaic system prograded into shallow water, lengthening the
392 longitudinal profile from 4 to 5.5 m. Initially, the system aggrades a wedge on the horizontal plane
393 while it becomes progradational from 4 h onwards, indicating it has reached a natural gradient along
394 the length of the initial horizontal plane. Compared to Scenario 1, the longitudinal profile of Scenario
395 2 remains more concave and maintains a substantially lower longitudinal gradient ([1:107] vs.
396 [1:180]), while sediment and water discharge were the same in both experiments (cf. Fig. 13A &
397 13D; Table 1). Grain-size data collected along the final longitudinal profile in Scenario 2 shows that
398 coarse-grained sand is preferentially retained in the relatively steep, upper reach of the profile (Fig.
399 13E). The lower reaches are relatively finer grained, indicating that this progradational system
400 effectively becomes finer downstream.

401

402 **5. CONTROLS ON FLUVIAL PROFILE SHAPE AND FLUVIO-MARINE SEDIMENT PARTITIONING**

403

5.1 Water depth in the receiving basin

404 With constant relative sea level, prograding systems cannot achieve system-scale
405 equilibrium (e.g. Fig. 6F, H; Fig 13D; Fig. 14A – D; Muto and Swenson 2005), due to aggradation along
406 the longitudinal profile. In shallow water conditions, such as occur at the start of E1_M1, E1_M2,
407 and in Scenario 2, fluvio-deltaic systems require limited sediment volumes deposited beyond the
408 shoreline to prograde rapidly. This results in strongly concave profiles at significantly lower gradients
409 than the equilibrium gradient, as indicated by a low fill and slope percentage of the longitudinal
410 profile (e.g. Fig. 6G, H; Fig. 7G, H, 0 – 48 h; Fig. 14B). Such systems transport sediment inefficiently
411 and deposit the bulk of their sediment load along the fluvio-deltaic topset (e.g. Fig. 7F, 0 – 48 h). The
412 progradation rates of fluvio-deltaic systems prograding into deep water are significantly lower and
413 allow the longitudinal profile to aggrade to a less concave and steeper gradient (i.e. approach the
414 equilibrium gradient; e.g. Fig. 6E, H, 48 – 96 h). Such systems transport sediment more efficiently
415 along the fluvio-deltaic topset and partition a significantly larger percentage of their sediment load
416 beyond the shoreline, where it becomes available for further redistribution in the marine domain
417 (Fig. 6F, 48 – 96 h; Fig. 14C).

418 Progradation will gradually slowdown in fluvio-deltaic systems that build a shelf clinoform
419 into a spatially deepening water body, such as ramp-style basin margins (e.g. Fig. 6C, E). A reduction
420 in the progradation rate allows the longitudinal profile to become steeper and less concave (Fig. 6G,
421 H; Fig. 14D), which increases the efficiency of sediment transport and enhances sediment transport
422 to beyond the shoreline (Fig. 6F; Fig. 14D). Therefore, a shift in the longitudinal sediment
423 partitioning can be expected in systems where the water depth (ie. shelf clinoform height) increases
424 spatially, over time depositing a smaller percentage of the sediment load in the fluvial and delta top
425 systems and more in the progradational delta front and slope clinoform successions (Fig. 6F; Fig.
426 14D). This process provides a potential mitigation mechanism for autoretreat (Muto 2001; Muto and
427 Steel 2002b) that is further discussed in the autostratigraphy paragraph.

428 Downstream sediment fining occurs in both gravel- and sand-bed rivers and is mainly
429 dependent on selective transport, although in gravel-bed rivers abrasion processes are important as
430 well (Frings 2008; Paola et al. 1992b). Selective transport is ineffective in longitudinal profiles that
431 are in system-scale equilibrium: fine-grained sand is more quickly transported than coarse-grained
432 sand but the latter will arrive as well, removing the downstream fining trend (Fig. 13A - C; Fig. 14A).

433 However, if a profile is below system-scale equilibrium, selective transport can result in stable
434 downstream fining trends (Fig. 13D, E; Fig. 14B, C) as a result of downstream decreases in bed shear
435 stress (Knighton 1999; Rice and Church 2001) or a downstream decrease in capacity to transport the
436 coarse grains by suspension transport (Frings 2008). In Scenario 1, a nearly linear longitudinal profile
437 develops after ~5.5 h. Longitudinal profiles at successive time steps overlap this profile, implying that
438 the system has aggraded to an approximate equilibrium gradient (Fig. 13A; Fig. 14A). This
439 approximately coincides with the arrival of coarse-grained sediment at the downstream weir in
440 similar quantities as in sediment input (Fig. 13C). Downstream fining has thus become ineffective,
441 which is further confirmed by the grain-size distribution along the final longitudinal profile (Fig. 13B;
442 Fig. 14A).

443 In Scenario 2, a progradational system developed with a low gradient, concave profile (Fig.
444 13D; Fig. 14B). Here, coarse-grained sand is retained in the steep upper reach of the fluvial profile,
445 indicating that the transport capacity at lower gradients is insufficient to transport the coarse
446 sediment fraction. Abrasion processes are insignificant in these models and the difference between
447 both experiments suggests that the downstream fining rate correlates with the concavity and
448 gradient of the longitudinal profile (e.g. Wright and Parker 2005a; Wright and Parker 2005b), that in
449 turn depend on progradation of the shoreline. The rate of progradation strongly depends on the
450 water depth of the receiving basin (e.g. Fig. 6; Fig. 7; Fig. 14B, C), which thus influences the
451 depositional character in the fluvial to marine domain and forms a downstream allogenic control on
452 both the volume and grain size of available sediment that can potentially be remobilized and
453 distributed into deeper marine environments (Fig. 14B – D).

454

455

5.2 Subsidence

456 E1_M2 examines the effects of water depth and subsidence. Shallow water progradation on
457 a non-subsiding substrate during the first half of the experiment allows for high progradation rates
458 in comparison to E1_M1 (cf. Fig. 7C, E & Fig. 6C, E). This results in a concave, low gradient
459 longitudinal profile (Fig. 7G, H) and results in low sediment volumes bypassing the shoreline (Fig. 7F;
460 Fig. 14B). The initiation of subsidence in the basin from 48 h onwards increases the water depth at
461 the shelf edge while generating substantial accommodation along the longitudinal profile, impeding
462 rapid progradation and maintaining low sediment bypass rates (Fig. 7). The reduced progradation
463 rate triggers a continuous increase in the gradient and a decrease in the concavity of the longitudinal
464 profile (Fig. 4A; Fig. 7G, H). From 80 h onwards, the sediment bypass volume beyond the shelf edge
465 increases to a higher level than that in the shallow non-subsiding basin, even though the high
466 subsidence rate is maintained (Fig. 7B, F). Subsidence therefore has two counteracting effects:
467 subsidence upstream of the shoreline generates accommodation and requires additional
468 sedimentation and potentially increases the concavity of the longitudinal profile (Sinha and Parker
469 1996). However, it also reduces the progradation rate by increased deposition on the topset and by
470 an increase in clinoform height, allowing the fluvio-deltaic system to more closely approach
471 equilibrium. In this experiment, progradation across a rapidly subsiding fluvio-deltaic topset (from 48
472 h onwards) was more efficient in bypassing sediment beyond the shelf edge than the shallow-water
473 system on a non-subsiding substrate (from 0 – 48 h) (Fig. 7F; Fig. 8C, D; Fig. 14D).

474

475

5.3 Sea level

476 In E2_M1, basal water-level variations are used to mimic glacio-eustatic sea-level
477 variations. These variations influence sedimentation in a basin that subsides at a constant rate (Fig.
478 9A, B), resulting in the progradation of a shelf clinoform in increasing water depths (e.g. Fig. 8E, F).
479 High-frequency sea-level variations form a strong additional control on the grade of the longitudinal
480 profile (e.g. Blum and Hattier-Womack 2009). As a first order approximation, a sequence-

481 stratigraphic interpretation based on relative sea-level variations alone provides a good explanation
482 for the stratigraphic stacking pattern (Fig. 8E, F). During sea-level rise, the downstream reaches of
483 the fluvio-deltaic system are aggradational and step back on the lowstand shelf (Fig. 11E). Sea-level
484 rise predominantly raises the lower reach of the longitudinal profile, resulting in a strongly concave
485 profile, shifted away from the system-scale equilibrium gradient (Fig. 9G, H; Fig. 14H). During relative
486 sea-level fall, the lower reaches of the longitudinal profile are eroded while deposition continues
487 upstream of sea-level influences (e.g. Fig. 12A). This generates a nearly linear profile that is close to
488 the system-scale equilibrium gradient (Fig. 9G, H; Muto and Swenson 2005) and results in efficient
489 sediment transport to the coastline (Fig. 9F; Fig. 14E, F). However, a relative sea-level-based
490 sequence-stratigraphic solution cannot explain why an incised valley only formed during the
491 moderate sea-level fall 3 (30 mm, Fig. 12C, 48 – 64 h), and not during the larger sea-level fall 1 (40
492 mm, Fig. 12A, 0 – 16 h).

493 Low shoreline progradation rates, in these experiments associated with deep water
494 conditions, lead to steeply descending shoreline trajectories during sea-level fall (Helland-Hansen
495 and Hampson 2009), steepening the longitudinal profile. Additionally, systems prograding into deep
496 water approach equilibrium conditions relatively closely compared to systems with higher
497 progradation rates (Fig. 6; Fig. 7). Combined, this allows systems to become strongly erosional locally
498 (Fig. 11; Fig. 12; Fig. 14G), a prerequisite for coastal incised-valley initiation (Strong and Paola 2008).
499 After valley incision, nearly all discharge is funneled through the incised valley. This causes an
500 increase in the water discharge per unit width, lowering the gradient at which the incised valley
501 system is in equilibrium (cf. Fig. 9H, 16 & 64 h), thereby triggering increased and prolonged erosion
502 (Fig. 9F; Fig. 14G). The latter is observed during sea-level fall 3, during which erosion migrates
503 upstream within a valley and persists till the following sea-level highstand (Fig. 12D). In this situation,
504 erosion has thus decoupled from sea-level fall and is maintained by the lowering of the fluvial
505 gradient within the incised valley, allowing for an increased diachroneity of the sequence boundary
506 (cf. Fig. 12B and Fig. 12D; Strong and Paola 2008).

507 A similar amplitude sea-level fall in shallow water systems will result in a more gradual
508 descending shoreline trajectory due to a higher progradation rate of the shoreline, causing the
509 longitudinal gradient to be further removed from system-scale equilibrium (Helland-Hansen and
510 Hampson 2009). Therefore, the rate of sea-level fall needs to be much more dramatic to steepen the
511 longitudinal profile sufficiently to surpass the equilibrium profile and trigger incision. Substantial
512 incision is thus less likely in shallow water systems, hindering the formation of incised valley systems.
513 If progradation rates are sufficiently high, systems might even remain aggradational during relative
514 sea-level fall. In E2_M2 for example, rapid progradation due to the exceptionally shallow water
515 conditions during sea-level fall 1 forces the fluvio-deltaic system away from equilibrium conditions,
516 while in other occurrences equilibrium is approached during sea-level fall (cf. Fig. 9 & Fig. 10). Such a
517 scenario might occur in shallow water systems or on wide shelves before sea level falls below shelf
518 edge. In such cases, the reduction of the longitudinal gradient might result in aggradation rather
519 than incision of the fluvio-deltaic succession even during sea-level fall (Ethridge et al. 1998; Petter
520 and Muto 2008; Prince and Burgess 2013; Swenson and Muto 2007; Wallinga et al. 2004). Water
521 depth thus strongly modulates the sensitivity of the fluvio-deltaic system to erosion induced by sea-
522 level fall and to the formation of incised valleys.

523 The incised valley of E2_M1 initiated in the deep zone of the experimental basin (Fig. 2; Fig.
524 11C) and we speculate that this is the most likely position, rather than lateral positions in the
525 shallow to intermediate depth zones. In depositional environments with lateral water depth
526 differences, the deep segments will require relatively longer time spans of fluvial activity to infill due
527 to the larger sediment volumes required. Additionally, the avulsion frequency of channels feeding
528 such segments might be reduced because avulsion frequency appears to be partially controlled by
529 the lengthening of the distributary channels (Edmonds et al. 2009), which will be slower due to
530 lower progradation rates. Therefore, it is likely that channels are present at positions feeding into

531 the deepest segments for prolonged periods, enhancing the probability of incision at such locations.
532 Such control on the lateral position of incised valleys within a depositional system is thought to be
533 relevant mainly when large lateral variations in water depth occur along short distances such as rift
534 basins.

535

536

5.4 *Water-sediment discharge ratio*

537 An increased water to sediment ratio results in more efficient sediment transport at lower
538 gradients (e.g. Simpson and Castelltort 2012), and can affect incised valley formation and style
539 (Bijkerk et al. 2013). This is also indicated by the differences between E2_M1 and E2_M2 (Fig. 8; Fig.
540 9; Fig. 10). The water to sediment ratio is 1.5 times higher in E2_M1 than in E2_M2. This resulted in
541 a ~1.2 times lower longitudinal gradient (see section 3.4 Dataset) and between 1 to 1.5 times higher
542 sediment bypass rates during sea-level fall (cf. Fig. 9F & Fig. 10F), implying significantly more
543 voluminous deposition in the delta front (cf. Fig. 8E, F & Fig. 8G, H). Additionally, higher water
544 discharge per unit width such as occurs in E2_M1 relative to E2_M2 results in shorter equilibrium
545 times (see section 3.3; Paola et al. 1992a), implying that a system will adapt more rapidly to
546 changing conditions such as relative sea-level fall. In E2_M1, these more favorable upstream
547 parameters resulted in lower concavity of the longitudinal profile and incised valley formation when
548 the experimental basin reached a sufficient depth during sea-level fall 3 (cf. Fig. 9G, H; Fig. 10G, H).
549 In E2_M2, the longitudinal profile remained significantly more concave, resulting in lower sediment
550 transport rates to the coastline and more deposition on the topset (Fig. 10F, G).

551

552

5.5 *Autostratigraphy*

553 Autostratigraphic principles (Muto et al. 2007) state that sedimentary systems influenced by
554 constant discharge and a constant rate of relative sea-level rise may transition from initial normal
555 regression, where sediment supply is still in excess of the accommodation creation, into
556 transgression or “autoretreat”. This is due to the increasing budget required to aggrade both slope
557 and topset of the sedimentary system (Muto 2001). At the autoretreat break, the increasing size of
558 the system reaches a tipping point at which sediment supply cannot support further progradation,
559 and 100% of the sediment load is partitioned to the topset. A subsequent increase in the topset area
560 due to landward onlap can cause the system to autoretreat (Muto and Steel 2002a).

561 The present results reveal an autoretreat mitigation mechanism. Progradation during
562 relative sea-level rise implies that the system builds out into increasing water depths, resulting in a
563 slowing of the progradation rate. The results suggest that this leads to an increase in the longitudinal
564 gradient and a reduction of its concavity (i.e. an increase in both the fill and slope percentage; Fig. 6;
565 Fig. 7), causing increasing rates of sediment bypass to beyond the shoreline. This enhanced sediment
566 transport efficiency increases the sediment volume available for progradation of the fluvio-deltaic
567 system, while it decreases the sediment volume that is used to for aggradation along the
568 longitudinal profile. This mechanism of increasing sediment bypass rates during progradation into
569 increasing water depths is well-illustrated in E1_M1 and E1_M2.

570 In E1_M1, the partitioning of sediment to beyond the shoreline doubles during progradation
571 into a basin of increasing water depth (Fig. 6C, F), despite a twofold increase in topset area (Fig. 6D)
572 (note that relative sea level is static and the water depth increase refers to a spatial increase). In
573 E1_M2, from 0 - 48 h a low gradient, strongly concave longitudinal system develops on a non-
574 subsiding substrate. Subsequently, a constant subsidence rate from 48 h onwards initially slows the
575 progradation rate due to the increase in accommodation along the longitudinal profile, and due to
576 the increasing water depth at the shelf edge (Fig. 7). This leads to a steepening of the longitudinal
577 gradient and a decrease in its concavity, which in turn results in increasing fluvial efficiency and
578 increasing sediment bypass towards the end of the experiment (Fig. 7). Whilst not excluding the

579 possibility of autoretreat, these results indicate that enhanced fluvial efficiency in routing sediment
580 beyond the shoreline as a consequence of increasing water depth may counter or delay its
581 occurrence.

582 From 56 h onwards, both the gradient and concavity of the E1_M1 longitudinal profile
583 remain constant (Fig. 6G, H) suggesting that the system has reached a balance between its approach
584 towards system-scale equilibrium conditions and the corresponding progradation related to the high
585 rates of sediment bypass to the shoreline. The constant gradient and concavity imply that the
586 increasing topset area (Fig. 6D) requires greater amounts of sediment, as is reflected in the slow
587 decrease in the sediment-bypass percentage (Fig. 6F). This suggests that when such balanced state is
588 attained, autostratigraphic principles might apply in a straightforward manner.

589

590

6. APPLICATION

591

592 The coupling of the system-scale equilibrium concept to shoreline progradation has been
593 used to explain that equilibrium on geologically relevant time scales can only be obtained during
594 relative sea-level fall, suggesting that sedimentary systems are generally not in equilibrium (Muto
595 and Swenson, 2005). The current analogue model dataset indicates that non-equilibrium results in a
596 broad spectrum of sediment partitioning trends along the longitudinal profile that might result in
597 variable stratigraphic patterns that are not related to allogenic forcing mechanisms, and becomes
598 predictable when related to water depth in the receiving basin.

599 Accommodation in fluvial settings is defined as the volume between the longitudinal profile
600 and the conceptual equilibrium profile (Posamentier and Allen 1999), and is closely related to
601 longitudinal patterns of sediment partitioning. The current results indicate that accommodation is
602 generally present in progradational systems without relative sea-level fluctuations, but that the infill
603 of such space becomes increasingly difficult when approaching the equilibrium profile (e.g. Fig. 6;
604 Fig. 13; Postma et al. 2008). Therefore, in slowly prograding systems that are close to equilibrium,
605 low rates of topset aggradation and high rates of sediment bypass beyond the shoreline can be
606 expected whereas in rapidly prograding systems the opposite occurs. In fluvial outcrops, such
607 different scenarios would be observed as either low- or high-accommodation style fluvial deposits,
608 although tectonic subsidence trends might be a more prominent cause. Gradual changes between
609 such low- or high-accommodation states are potentially related to changing water depth and do not
610 necessarily relate to relative sea-level variations or variable subsidence rates in the fluvial domain.

611 In the deltaic domain, the arrival of increasing volumes and grain sizes might be coupled to
612 the arrival of the shelf edge in deep water, where it can trigger increasing activity of linked turbidite
613 systems (e.g. Nelson et al. 2009). Therefore, knowledge of water depth and associated progradation
614 rates might help interpret and predict stratigraphic trends in both the fluvial, deltaic and marine
615 domains.

616 Based on these experiments, stratigraphic trends related to the efficiency of sediment
617 transport along the longitudinal profile are likely present in shelf clinoforms. The importance of such
618 trends in natural systems relative to other upstream factors such as changes in the sediment or
619 water discharge, for example due to tectonic or climate regime, or downstream controls such as
620 relative sea level has yet to be determined. Effects might be obscured if small or misinterpreted if
621 significant. Additional work on shelf clinoform successions will be required to determine the relative
622 importance in different settings. Based on literature review two case studies of shelf margin
623 successions are selected that demonstrate aspects of these analogue models in natural systems.
624 Both case studies, the Maastrichtian Lance - Fox Hills - Lewis shelf margin of Southern Wyoming and
625 the Eocene Central Basin of Spitsbergen have relatively small, mountainous catchment areas and
626 prograde for several 10's of kilometers into basins with water depths of several hundreds of meters.

627 Such small sedimentary systems respond relatively quickly, making it more likely that the variations
628 in the grade of the longitudinal profile are recorded recognizably in the stratigraphic record.

629 *6.1 Case study 1: The Maastrichtian Lance - Fox Hills - Lewis shelf margin, Southern Wyoming*

630 The Maastrichtian Lance - Fox Hills - Lewis shelf margin of Southern Wyoming is a well-
631 studied shelf-margin succession that can be used to test the concepts from analogue modeling in a
632 setting that is not influenced by high-amplitude, high-frequency glacio-eustatic variation (e.g. Miller
633 et al., 2005; Carvajal, 2007), analogous to Experiment 1 in this study.

634 Over a period of 1 to 1.5 Myr, rapid shelf-margin accretion resulted in the formation of 15
635 clinothems (Carvajal 2007; Carvajal and Steel 2012; Carvajal and Steel 2009; Carvajal and Steel 2006)
636 that can be subdivided into two stages. The first stage was deposited in a rapidly subsiding basin and
637 is represented by clinothems C0-C9 (Fig. 15A). Based on the gradually but irregularly rising shelf-
638 edge trajectory, an overall water depth increase from ~250 to >400 m is recorded. Subsidence was
639 directly linked to Laramide tectonic activity across the region, triggering subsidence in the basin and
640 uplift in its source area (Carvajal, 2007; Carvajal and Steel 2012). Stage 2, represented by clinothems
641 C10-15, initiates when active thrusting and uplift in the source area had decreased or ceased
642 (Carvajal, 2007). These clinothems form a progradational succession in a basin of fairly constant
643 depth, as reflected by the low-angle to horizontal shelf-edge trajectory (Fig. 15A; Carvajal and Steel
644 2006).

645 The average sediment supply rate calculated for Stage 1 is $\sim 4 - 10 * 10^6$ ton / yr; the
646 progradational succession of Stage 2 has a higher sediment supply rate of $8 - 16 * 10^6$ ton / yr during
647 a period of tectonic inactivity (Carvajal 2007; Carvajal and Steel 2012). The increase in sediment
648 supply from Stage 1 to Stage 2 is counter-intuitive since the decreasing rate of thrusting in the
649 source area is expected to correspond to a decrease in the sediment yield. The increase in sediment
650 yield is therefore linked to modest uplift due to isostatic rebound, persistence of high relief, and
651 increasing catchment area (Carvajal 2007; Carvajal and Steel 2012). Additionally, the overall
652 sand/shale ratio increases over time, which has been ascribed to erosion of increasingly sandy
653 source rock, documented from the stratigraphy of the region (Fig. 15B; Carvajal 2007; Carvajal and
654 Steel 2012).

655 As an additional hypothesis, we suggest that the progressive increase in water depth during
656 Stage 1 and the near-cessation of relative sea-level rise at the transition from Stage 1 to Stage 2 can
657 contribute to the increase in sediment volume and the increase in sand/shale ratio. The sea-level
658 stillstand and increased water depth allow the longitudinal profile to grade closer towards
659 equilibrium (Fig. 15C). This enhances the sediment bypass rate and allows transport of coarser
660 sediment into the basin, which increases the sand/shale ratio in both the basin floor, and overall
661 (Fig. 15B).

662 *6.2 Case study 2: Eocene Central Basin, Spitsbergen*

663 The Eocene Central Basin of Spitsbergen provides one of very few outcrops of well-
664 preserved shelf-margin clinothem complexes, from coastal plains to deepwater fans. Sea-level
665 cyclicity is estimated at ~300 kyr duration (Crabaugh and Steel 2004). Two contrasting shelf-margin
666 types, Type I and II, developed broadly at the same period within the region (Plink-Björklund and
667 Steel 2005) and demonstrate the influence of basin depth and progradation rate on incised valley
668 formation.

669 Type I shelf margins are characterized by severe erosion of the outer shelf by falling stage
670 shelf-edge deltas, accompanied by the formation of significant basin floor fans that are fed from
671 across a disrupted slope (Plink-Björklund and Steel 2005). Shelf margin accretion occurs mainly
672 during the late lowstand and occurs in water depths of 300 – 350 m (Plink-Björklund and Steel 2005;
673 Steel et al. 2007). Type II shelf margins are characterized by the absence of a basin floor fan and
674 accrete with an amalgamated succession of falling stage, early and late lowstand deltas. Falling stage

675 deltas are notably highly progradational. Of Type II margins, only the Reindalen clinothems (26-27)
676 show complete exposures including the clinothem top. In these clinothems, water depth is
677 estimated at ~200 m (Plink-Björklund and Steel 2002; Plink-Björklund and Steel 2005; Plink-Björklund
678 and Steel 2007).

679 Both clinothem types are broadly coeval, and eustatic sea level is interpreted to fall below
680 the shelf edge in both shelf-margin styles (Plink-Björklund and Steel 2005). Therefore, the different
681 character is dependent on other inherent characteristics of these shelf types. Plink-Björklund and
682 Steel (2005), suggest that higher sediment/water discharges and higher rates of sediment fallout at
683 the shelf-edge and upper slope during the falling stage in Type II shelf margins dampens incision and
684 prevents deep channeling at the shelf edge. Alternatively, the shallow water depth of Type II
685 clinothems facilitates higher progradation rates, impeding incision due to the resultant lower
686 gradient of the descending shoreline trajectory (cf. Fig. 7E, F, 0 – 16 h; Fig. 14E; Holbrook et al.
687 2006). Type I clinothems formed in deeper basins and are characterized by slower progradation
688 rates, resulting in a slightly steeper downward-directed shoreline trajectory with the same rate of
689 sea-level fall. This causes the longitudinal profile to become above grade and allows for sufficient
690 shelf incision to generate incised feeder channels (cf. Fig. 7E, F, 48 – 64 h; Fig. 14G; Strong and Paola
691 2008). Consequently, the likelihood of shelf incision during sea-level fall increases with water depth
692 in the receiving basin, resulting in the different development of Type I and Type II deltas. Dependent
693 on the water depth, both the timing of shelf margin progradation differs and the gross architecture
694 of shelf clinof orm is altered.

695

696

697

7. CONCLUSIONS

698 Analogue modeling is used to examine the impact of basinal water depth, and downstream
699 allogenic controls on the temporal development of the longitudinal profile of progradational fluvio-
700 deltaic systems and associated small-scale shelf margins. Analyses focus on the relationship between
701 the gradient and concavity of the longitudinal profile and the corresponding sediment transport
702 efficiency. System-scale equilibrium is defined as an end member and represents a state in which the
703 longitudinal profile does not change shape while all sediment is bypassed beyond the shoreline.
704 With constant relative sea level, progradational fluvio-deltaic systems develop towards but cannot
705 reach this state because lengthening of the longitudinal profile requires continuous aggradation
706 along the longitudinal profile. This implies that the departure from system-scale equilibrium is
707 governed by the progradation rate. Water depth, subsidence, and sea-level variations act as
708 allogenic controls on the migration of the shoreline, thus affecting how closely the fluvio-deltaic
709 profile approaches equilibrium, thereby controlling the development of the longitudinal profile and
710 fluvial to marine sediment partitioning.

711 Shallow water depth results in rapid lengthening of the sedimentary system. This causes a
712 strongly concave, low gradient longitudinal profile that is associated with high aggradation rates in
713 the fluvial domain and strong downstream fining trend. In deep water systems, shoreline
714 progradation rates are significantly lower, allowing the longitudinal profile of sedimentary systems
715 to steepen and approach equilibrium more closely. This results in limited accommodation in the
716 fluvial domain and high sediment supply to the shoreline with limited downstream fining. Increasing
717 water depths, for example in ramp-style basins, reduce the progradation rate and therefore
718 gradually shift the partitioning of sediment from mainly fluvial towards predominantly marine
719 deposition. Water depth, through its effect on progradation rates, thus influences the sediment
720 partitioning of sedimentary systems and forms a first order control on the availability of sand-rich
721 sediments that can potentially be remobilized and redistributed into deeper marine environments.

722 Subsidence has a dual effect: it generates accommodation along the longitudinal profile
723 limiting sediment transport to the shoreline. Counterintuitively, the resultant slow progradation
724 rates can allow the fluvio-deltaic system to grade towards equilibrium which can eventually increase
725 the sediment transport efficiency along the longitudinal profile.

726 Relative sea-level variations rapidly alter the fluvio-deltaic longitudinal gradient. In deep
727 water systems, low shoreline progradation rates result in steep descending shoreline trajectories
728 during relative sea-level fall, generating significantly greater erosion than in shallow water systems.
729 Deep water conditions therefore result in higher sediment yields beyond the shoreline and an
730 increased probability of incised valley formation. The latter can alter the timing of shelf margin
731 progradation and its gross morphology and therefore affect the transfer of sediment to deep marine
732 sinks. The experimental results indicate that, during glacio-eustatic sea-level cyclicity, the
733 longitudinal profile is closest to equilibrium during relative sea-level fall and early lowstand. This
734 results in efficient sediment transport towards the shoreline, explaining delivery of increased
735 sediment volumes of increasing grain size to lowstand systems tracts as a relative sea level and
736 water-depth-controlled parameter.

737

738

8. ACKNOWLEDGEMENTS

739 This work is in part funded by a BGS University Funding Initiative PhD studentship (BUFI
740 S194) to J.B., sponsors of the Turbidites Research Group, and the University of Leeds. We are
741 grateful to Thony van Gon Netscher, Henk van der Meer and Dineke Wiersma for support during the
742 experiments. We thank Michael Ellis and Oliver Wakefield for their comments on an earlier version
743 of the manuscript. Suggestions from reviewers Ron Steel, Jacob Covault, Cristian Carvajal, and JSR
744 editor Tobi Payenberg greatly improved the manuscript. J.B. and C.N.W. publish with the permission
745 of the Executive Director, British Geological Survey, Natural Environment Research Council.

746

747

9. REFERENCES

- 748 BIJKERK, J.F., 2014, External Controls on Sedimentary Sequences: a Field and Analogue Modelling
749 Based Study [unpublished PhD thesis]: University of Leeds, Leeds, 259 p.
- 750 BIJKERK, J.F., POSTMA, G., TEN VEEN, J., MIKES, D., VAN STRIEN, W., and DE VRIES, J., 2013, The role
751 of climate variation in delta architecture: lessons from analogue modelling: Basin Research,
752 v. 25, p. 1-18.
- 753 BLUM, M., and HATTIER-WOMACK, J., 2009, Climate change, sea-level change, and fluvial sediment
754 supply to deepwater depositional systems, in Kneller, B., Martinsen, O.J., and McCaffrey,
755 W.D., eds., External Controls on Deep Water Depositional Systems, SEPM Special
756 Publication, v. 92, p. 15-39.
- 757 BOURGET, J., ZARAGOSI, S., RODRIGUEZ, M., FOURNIER, M., GARLAN, T., and CHAMOT-ROOKE, N.,
758 2013, Late Quaternary megaturbidites of the Indus Fan: Origin and stratigraphic significance:
759 Marine Geology, v. 336, p. 10-23.
- 760 CARVAJAL, C., 2007, Sediment volume partitioning, topset processes and clinoform architecture -
761 understanding the role of sediment supply, sea level, and delta types in shelf margin building
762 and deepwater sand bypass: the Lance-Fox Hills-Lewis system in S. Wyoming [unpublished
763 PhD thesis]: The University of Texas at Austin, 171 p.
- 764 CARVAJAL, C., and STEEL, R., 2012, Source-to-sink sediment volumes within a tectono-stratigraphic
765 model for a Laramide shelf-to-deep-water basin: methods and results, in Busby, C., and Azor,
766 A., eds., Tectonics of Sedimentary Basins, Blackwell Publishing Ltd., p. 131-151.

- 767 CARVAJAL, C., and STEEL, R., 2009, Shelf-Edge Architecture and Bypass of Sand to Deep Water:
768 Influence of Shelf-Edge Processes, Sea Level, and Sediment Supply: *Journal of Sedimentary*
769 *Research*, v. 79, p. 652-672.
- 770 CARVAJAL, C.R., and STEEL, R.J., 2006, Thick turbidite successions from supply-dominated shelves
771 during sea-level highstand: *Geology*, v. 34, p. 665-668.
- 772 CASTELLTORT, S., and VAN DEN DRIESSCHE, J., 2003, How plausible are high-frequency sediment
773 supply-driven cycles in the stratigraphic record?: *Sedimentary Geology*, v. 157, p. 3-13.
- 774 CATUNEANU, O., ABREU, V., BHATTACHARYA, J.P., BLUM, M.D., DALRYMPLE, R.W., ERIKSSON, P.G.,
775 FIELDING, C.R., FISHER, W.L., GALLOWAY, W.E., GIBLING, M.R., GILES, K.A., HOLBROOK, J.M.,
776 JORDAN, R., KENDALL, C.G.S.C., MACURDA, B., MARTINSEN, O.J., MIALL, A.D., NEAL, J.E.,
777 NUMMEDAL, D., POMAR, L., POSAMENTIER, H.W., PRATT, B.R., SARG, J.F., SHANLEY, K.W.,
778 STEEL, R.J., STRASSER, A., TUCKER, M.E., and WINKER, C., 2009, Towards the standardization
779 of sequence stratigraphy: *Earth-Science Reviews*, v. 92, p. 1-33.
- 780 COVAULT, J.A., ROMANS, B.W., GRAHAM, S.A., FILDANI, A., and HILLEY, G.E., 2011, Terrestrial source
781 to deep-sea sink sediment budgets at high and low sea levels: Insights from tectonically
782 active Southern California: *Geology*, v. 39, p. 619-622.
- 783 CRABAUGH, J.P., and STEEL, R.J., 2004, Basin-floor fans of the Central Tertiary Basin, Spitsbergen:
784 relationship of basin-floor sand-bodies to prograding clinoforms in a structurally active
785 basin, in Lomas, S.A., and Joseph, P., eds., *Confined Turbidite Systems*, Geological Society,
786 London, Special Publications, v.222, p. 187-208.
- 787 EDMONDS, D.A., HOYAL, D.C.J.D., SHEETS, B.A., and SLINGERLAND, R.L., 2009, Predicting delta
788 avulsions: Implications for coastal wetland restoration: *Geology*, v. 37, p. 759-762.
- 789 ETHRIDGE, F.G., WOOD, L.J., and SCHUMM, S.A., 1998, Cyclic variables controlling fluvial sequence
790 development: Problems and perspectives, in Shanley, K.W., and McCabe, P.W., eds., *Relative*
791 *Role of Eustasy, Climate, and Tectonism in Continental Rocks*, SEPM Special Publication, v.
792 59, p. 17-29.
- 793 FRINGS, R.M., 2008, Downstream fining in large sand-bed rivers: *Earth-Science Reviews*, v. 87, p. 39-
794 60.
- 795 HAMPSON, G.J., JEWELL, T.O., IRFAN, N., GANI, M.R., and BRACKEN, B., 2013, Modest Change In
796 Fluvial Style With Varying Accommodation In Regressive Alluvial-To-Coastal-Plain Wedge:
797 Upper Cretaceous Blackhawk Formation, Wasatch Plateau, Central Utah, U.S.A: *Journal of*
798 *Sedimentary Research*, v. 83, p. 145-169.
- 799 HELLAND-HANSEN, W., and HAMPSON, G.J., 2009, Trajectory analysis: concepts and applications:
800 *Basin Research*, v. 21, p. 454-483.
- 801 HELLAND-HANSEN, W., STEEL, R.J., and SØMME, T.O., 2012, Shelf genesis revisited: *Journal of*
802 *Sedimentary Research*, v. 82, p. 133-148.
- 803 HOLBROOK, J., SCOTT, R.W., and OBOH-IKUENOBE, F.E., 2006, Base-level buffers and buttresses: A
804 model for upstream versus downstream control on fluvial geometry and architecture within
805 sequences: *Journal of Sedimentary Research*, v. 76, p. 162-174.
- 806 HOLBROOK, J.M., and BHATTACHARYA, J.P., 2012, Reappraisal of the sequence boundary in time and
807 space: Case and considerations for an SU (subaerial unconformity) that is not a sediment
808 bypass surface, a time barrier, or an unconformity: *Earth-Science Reviews*, v. 113, p. 271-
809 302.
- 810 KIM, W., and PAOLA, C., 2007, Long-period cyclic sedimentation with constant tectonic forcing in an
811 experimental relay ramp: *Geology*, v. 35, p. 331.

- 812 KIM, W., PAOLA, C., VOLLER, V.R., and SWENSON, J.B., 2006, Experimental Measurement of the
813 Relative Importance of Controls on Shoreline Migration: *Journal of Sedimentary Research*, v.
814 76, p. 270-283.
- 815 KNIGHTON, A.D., 1999, Downstream variation in stream power: *Geomorphology*, v. 29, p. 293-306.
- 816 KOSS, J.E., ETHRIDGE, F.G., and SCHUMM, S.A., 1994, An Experimental-Study of the Effects of Base-
817 Level Change on Fluvial, Coastal-Plain and Shelf Systems: *Journal of Sedimentary Research*
818 Section B-Stratigraphy and Global Studies, v. 64, p. 90-98.
- 819 LISIECKI, L.E., and RAYMO, M.E., 2005, A Pliocene-Pleistocene stack of 57 globally distributed benthic
820 $d^{18}O$ records: *Paleoceanography*, v. 20, p. PA1003.
- 821 MACKIN, J.H., 1948, Concept of the Graded River: *Geological Society of America Bulletin*, v. 59, p.
822 463-512.
- 823 MARTIN, J., CANTELLI, A., PAOLA, C., BLUM, M., and WOLINSKY, M., 2011, Quantitative Modeling of
824 the Evolution and Geometry of Incised Valleys: *Journal of Sedimentary Research*, v. 81, p. 64-
825 79.
- 826 MARTINSEN, O.J., COLLINSON, J.D., and HOLDSWORTH, B.K., 1995, Millstone Grit Cyclicity Revisited,
827 II: Sequence Stratigraphy and Sedimentary Responses to Changes of Relative Sea-Level, in
828 Plint, A.G., ed., *Sedimentary Facies Analysis*, Blackwell Publishing Ltd., p. 305-327.
- 829 MARTINSEN, O.J., SØMME, T.O., THURMOND, J.B., HELLAND-HANSEN, W., and LUNT, I., 2010,
830 Source-to-sink systems on passive margins: theory and practice with an example from the
831 Norwegian continental margin, in Vining, B.A., and Pickering, S.C., eds., *Petroleum Geology:*
832 *From Mature Basins to New Frontiers – Proceedings of the 7th Petroleum Geology*
833 *Conference*, Geological Society, London, *Petroleum Geology Conference series*, v. 7, p. 913-
834 920.
- 835 MIALL, A.D., 2013, *Fluvial Depositional Systems*: Berlin, Springer, 316 p.
- 836 MUTO, T., 2001, Shoreline autoretreat substantiated in flume experiments: *Journal of Sedimentary*
837 *Research*, v. 71, p. 246-254.
- 838 MUTO, T., and STEEL, R.J., 2002a, In Defense of Shelf-Edge Delta Development during Falling and
839 Lowstand of Relative Sea Level: *Journal of Geology*, v. 110, p. 421-436.
- 840 MUTO, T., and STEEL, R.J., 2002b, Role of autoretreat and AS changes in the understanding of deltaic
841 shoreline trajectory: a semi-quantitative approach: *Basin Research*, v. 14, p. 303-318.
- 842 MUTO, T., STEEL, R.J., and SWENSON, J.B., 2007, Autostratigraphy: A framework norm for genetic
843 stratigraphy: *Journal of Sedimentary Research*, v. 77, p. 2-12.
- 844 MUTO, T., and SWENSON, J.B., 2005, Large-scale fluvial grade as a nonequilibrium state in linked
845 depositional systems: Theory and experiment: *Journal of Geophysical Research: Earth*
846 *Surface*, v. 110, p. F03002.
- 847 MUTO, T., and SWENSON, J.B., 2006, Autogenic attainment of large-scale alluvial grade with steady
848 sea-level fall: An analog tank-flume experiment: *Geology*, v. 34, p. 161.
- 849 NELSON, C.H., ESCUTIA, C., GOLDFINGER, C., KARABONOV, E., GUTIERREZ-PASTOR, J., and DE BATIST,
850 M., 2009, External Controls On Modern Clastic Turbidite Systems: Three Case Studies, in
851 Kneller, B., Martinsen, O.J., and McCaffrey, W.D., eds., *External Controls on Deep-Water*
852 *Depositional Systems*, SEPM Special Publication, v. 92, p. 57-76.
- 853 OHMORI, H., 1991, Change in the Mathematical Function Type Describing the Longitudinal Profile of
854 a River through an Evolutionary Process: *The Journal of Geology*, v. 99, p. 97-110.

- 855 PAOLA, C., HELLER, P.L., and ANGEVINE, C.L., 1992a, The large-scale dynamics of grain-size variation
856 in alluvial basins, 1: Theory: Basin Research, v. 4, p. 73-90.
- 857 PAOLA, C., PARKER, G., SEAL, R., SINHA, S.K., SOUTHARD, J.B., and WILCOCK, P.R., 1992b,
858 Downstream Fining by Selective Deposition in a Laboratory Flume: Science, v. 258, p. 1757-
859 1760.
- 860 PAOLA, C., STRAUB, K., MOHRIG, D., and REINHARDT, L., 2009, The "unreasonable effectiveness" of
861 stratigraphic and geomorphic experiments: Earth-Science Reviews, v. 97, p. 1-43.
- 862 PETTER, A.L., and MUTO, T., 2008, Sustained alluvial aggradation and autogenic detachment of the
863 alluvial river from the shoreline in response to steady fall of relative sea level: Journal of
864 Sedimentary Research, v. 78, p. 98-111.
- 865 PLINK-BJÖRKLUND, P., and STEEL, R., 2002, Sea-level fall below the shelf edge, without basin-floor
866 fans: Geology, v. 30, p. 115-118.
- 867 PLINK-BJÖRKLUND, P., and STEEL, R., 2005, Deltas on Falling-Stage and Lowstand Shelf Margins, The
868 Eocene Central Basin of Spitsbergen: Importance of Sediment Supply, in Giosan, L., and
869 Bhattacharya, J., eds., River Deltas-Concepts, Models, and Examples, SEPM Special
870 Publication, v. 83, p. 179-206.
- 871 PLINK-BJÖRKLUND, P., and STEEL, R., 2006, Incised valleys on a Eocene coastal plain and shelf,
872 Spitsbergen - part of a linked shelf-slope system, in Dalrymple, R.W., Leckie, D.A., and
873 Tillman, R.W., eds., Incised Valleys in Time and Space: SEPM Spec. Publ. 85, SEPM Spec. Publ.
874 85.
- 875 PLINK-BJÖRKLUND, P., and STEEL, R., 2007, Type II Shelf Margin, Hogsnyta, Norway: Attached Slope
876 Turbidite System, in Nilsen, T.H., Shew, R.D., Steffens, G.S., and Studlick, J.R.J., eds., Atlas of
877 Deep-Water Outcrops: American Association of Petroleum Geologists, Studies in Geology 56,
878 p. 282-286.
- 879 POSAMENTIER, H.W., and ALLEN, G.P., 1999, Fundamental Concepts of Sequence Stratigraphy,
880 Siliciclastic Sequence Stratigraphy—Concepts and Applications, SEPM Concepts in
881 Sedimentology and Paleontology 7, p. 9-51.
- 882 POSAMENTIER, H.W., and JAMES, D.P., 1993, An Overview of Sequence-Stratigraphic Concepts: Uses
883 and Abuses: Sequence Stratigraphy and Facies Associations, Blackwell Publishing Ltd., 1-18
884 p.
- 885 POSAMENTIER, H.W., and VAIL, P.R., 1988, Eustatic controls on clastic deposition II - sequence and
886 system tract models, in Wilgus, C.K., Hastings, B.S., Kendall, C.G.S.C., Posamentier, H.W.,
887 Ross, H.W., and Van Wagoner, J.C., eds., Sea Level Changes - An Integrated Approach, SEPM
888 Special Publication, v. 42, p. 125-154.
- 889 POSTMA, G., KLEINHANS, M.G., MEIJER, P.T., and EGGENHUISEN, J.T., 2008, Sediment transport in
890 analogue flume models compared with real-world sedimentary systems: a new look at
891 scaling evolution of sedimentary systems in a flume: Sedimentology, v. 55, p. 1541-1557.
- 892 PRINCE, G.D., and BURGESS, P.M., 2013, Numerical Modeling of Falling-Stage Topset Aggradation:
893 Implications for Distinguishing Between Forced and Unforced Regressions In the Geological
894 Record: Journal of Sedimentary Research, v. 83, p. 767-781.
- 895 RICE, S.P., and CHURCH, M., 2001, Longitudinal profiles in simple alluvial systems: Water Resources
896 Research, v. 37, p. 417-426.
- 897 SCHUMM, S.A., and LICHTY, R.W., 1965, Time, space, and causality in geomorphology: American
898 Journal of Science, v. 263, p. 110-119.

- 899 SHANLEY, K.W., and MCCABE, P.J., 1994, Perspectives on the Sequence Stratigraphy of Continental
900 Strata: AAPG Bulletin, v. 78, p. 544-568.
- 901 SIMPSON, G., and CASTELLORT, S., 2012, Model shows that rivers transmit high-frequency climate
902 cycles to the sedimentary record: *Geology*, v. 40, p. 1131-1134.
- 903 SINHA, S.K., and PARKER, G., 1996, Causes of Concavity in Longitudinal Profiles of Rivers: *Water
904 Resources Research*, v. 32, p. 1417-1428.
- 905 SNOW, R.S., and SLINGERLAND, R.L., 1987, Mathematical Modeling of Graded River Profiles: *The
906 Journal of Geology*, v. 95, p. 15-33.
- 907 SØMME, T.O., HELLAND-HANSEN, W., and GRANJEON, D., 2009, Impact of eustatic amplitude
908 variations on shelf morphology, sediment dispersal, and sequence stratigraphic
909 interpretation: *Icehouse versus greenhouse systems: Geology*, v. 37, p. 587-590.
- 910 STEEL, R., PLINK-BJÖRKLUND, P., and MELLERE, D., 2007, Storvola, Type I Shelf Margin, Norway, in
911 Nilsen, T.H., Shew, R.D., Steffens, G.S., and Studlick, J.R.J., eds., *Atlas of Deep-Water
912 Outcrops: American Association of Petroleum Geologists, Studies in Geology* 56, p. 274-281.
- 913 STRONG, N., and PAOLA, C., 2008, Valleys that never were: time surfaces versus stratigraphic
914 surfaces: *Journal of Sedimentary Research*, v. 78, p. 579-593.
- 915 SWENSON, J.B., and MUTO, T., 2007, Response of coastal plain rivers to falling relative sea-level:
916 allogenic controls on the aggradational phase: *Sedimentology*, v. 54, p. 207-221.
- 917 VAN HEIJST, M., POSTMA, G., VAN KESTEREN, W.P., and DE JONGH, R.G., 2002, Control of
918 syndepositional faulting on systems tract evolution across growth faulted shelf margins: An
919 analog experimental model of the Miocene Imo River field, Nigeria: *AAPG Bulletin*, v. 86, p.
920 1335-1366.
- 921 VAN HEIJST, M.W.I.M., and POSTMA, G., 2001, Fluvial response to sea-level changes: a quantitative
922 analogue, experimental approach: *Basin Research*, v. 13, p. 269-292.
- 923 VOLLER, V.R., and PAOLA, C., 2010, Can anomalous diffusion describe depositional fluvial profiles?:
924 *Journal of Geophysical Research: Earth Surface*, v. 115, p. F00A13.
- 925 VOLLMER, S., and KLEINHANS, M.G., 2007, Predicting incipient motion, including the effect of
926 turbulent pressure fluctuations in the bed: *Water Resources Research*, v. 43, p. W05410.
- 927 WALLINGA, J., TÖRNQVIST, T.E., BUSSCHERS, F.S., and WEERTS, H.J.T., 2004, Allogenic forcing of the
928 late Quaternary Rhine–Meuse fluvial record: the interplay of sea-level change, climate
929 change and crustal movements: *Basin Research*, v. 16, p. 535-547.
- 930 WHEELER, H.E., 1964, Baselevel, Lithosphere Surface, and Time-Stratigraphy: *Geological Society of
931 America Bulletin*, v. 75, p. 599-610.
- 932 WRIGHT, S., and PARKER, G., 2005a, Modeling downstream fining in sand-bed rivers. I: formulation:
933 *Journal of Hydraulic Research*, v. 43, p. 613-620.
- 934 WRIGHT, S., and PARKER, G., 2005b, Modeling downstream fining in sand-bed rivers. II: application:
935 *Journal of Hydraulic Research*, v. 43, p. 621-631.
- 936
- 937
- 938
- 939
- 940

941

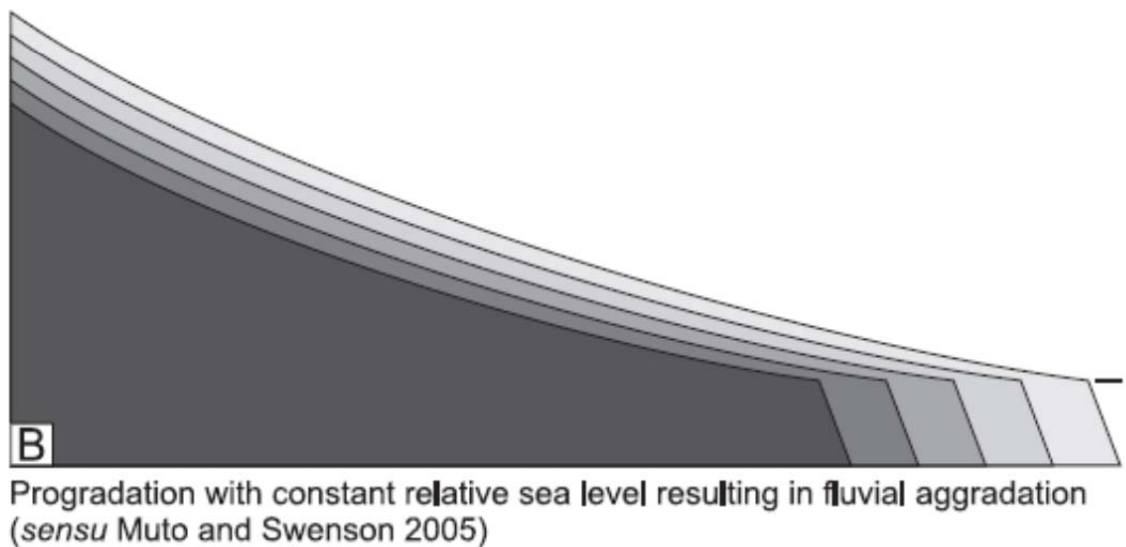
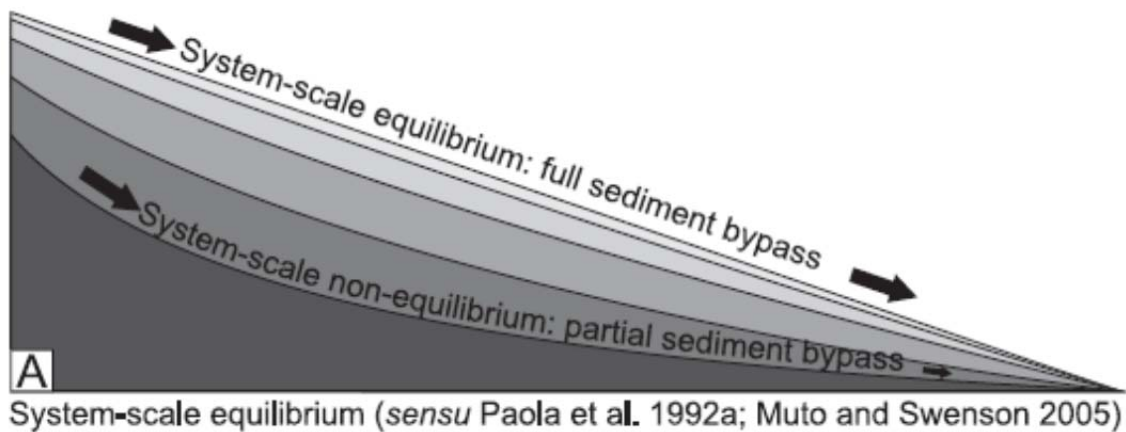
942

9. FIGURE CAPTIONS

	Q_w ($m^3 h^{-1}$)	Q_s ($m^3 h^{-1}$)	T (h)	ΔT (h)	Boundary Conditions Varied
E1_M1	1	0.004	96	8	Water depth
E1_M2	1	0.004	96	8	Water depth and subsidence
E2_M1	1.5	0.004	72	8	Water depth, subsidence, and sea-level variation
E2_M2	1	0.004	72	8	Water depth, subsidence, and sea-level variation
Scenario 1	5.5	0.007	8	0.5	Basin with constraining weir, no progradation
Scenario 2	5.5	0.007	8	0.5	Shallow-water progradation (3 cm)

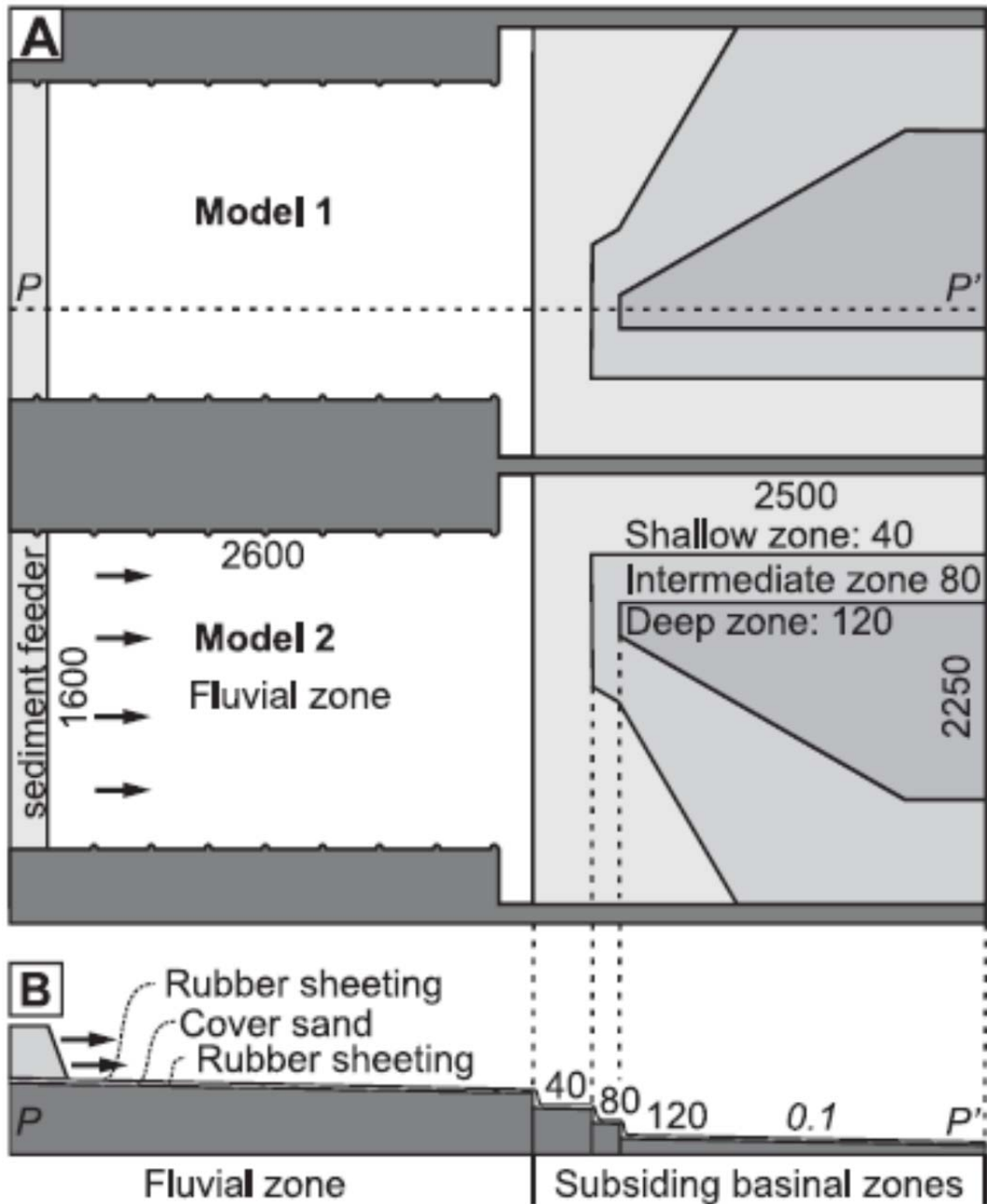
943

944 Table 1: Input parameters and boundary conditions of the experiments. Q_w and Q_s denote water and
 945 sediment discharge, respectively. T and ΔT , denote the duration of the experiment and the interval
 946 between measurements.



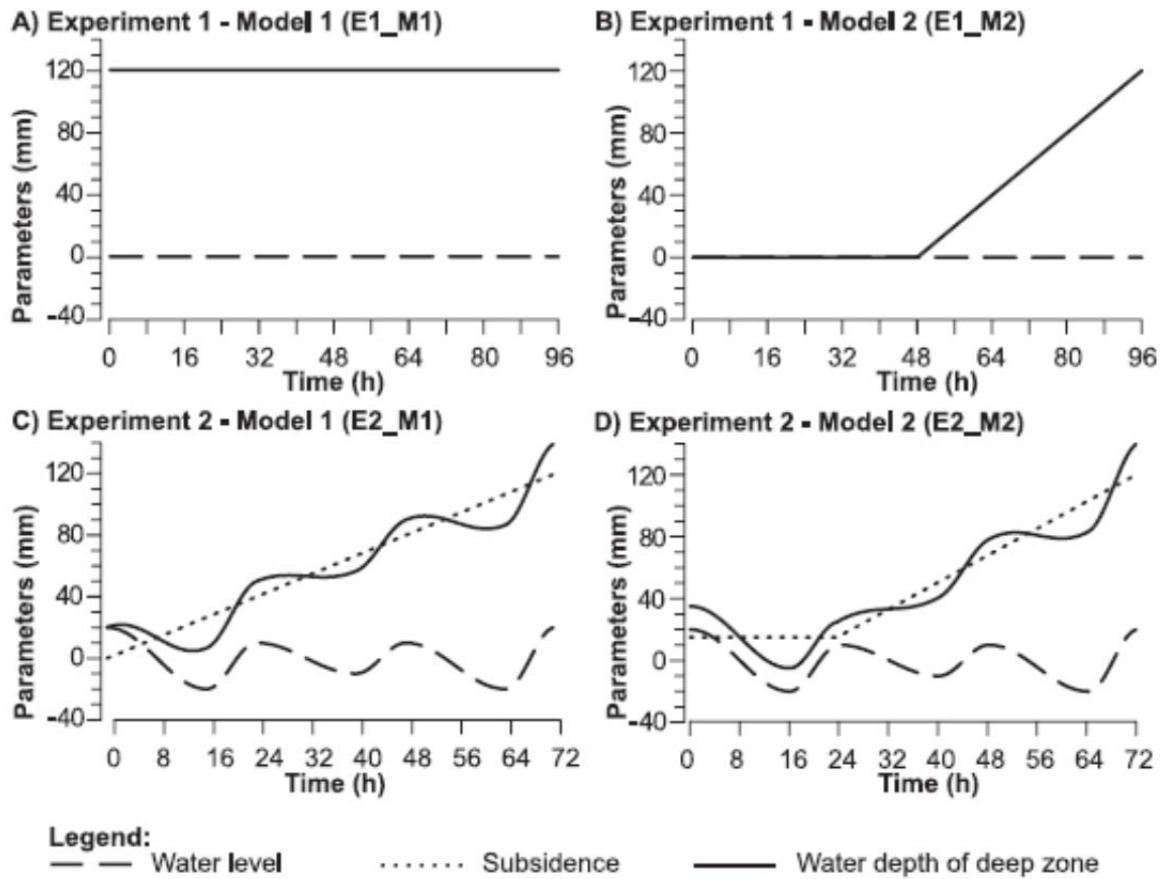
947

948 FIG. 1: (A) System-scale equilibrium (*sensu* Paola et al. 1992a) is only obtained over geological time
 949 scales. The linear equilibrium profile drawn here is idealized (cf. Postma et al. 2008) and will not
 950 form in natural systems for multiple reasons but illustrates that all fluvial accommodation is infilled.
 951 (B) Development of fluvio-deltaic systems on geological time scales. Progradation results in
 952 aggradation along the longitudinal profile and prevents these systems from achieving system-scale
 953 equilibrium.



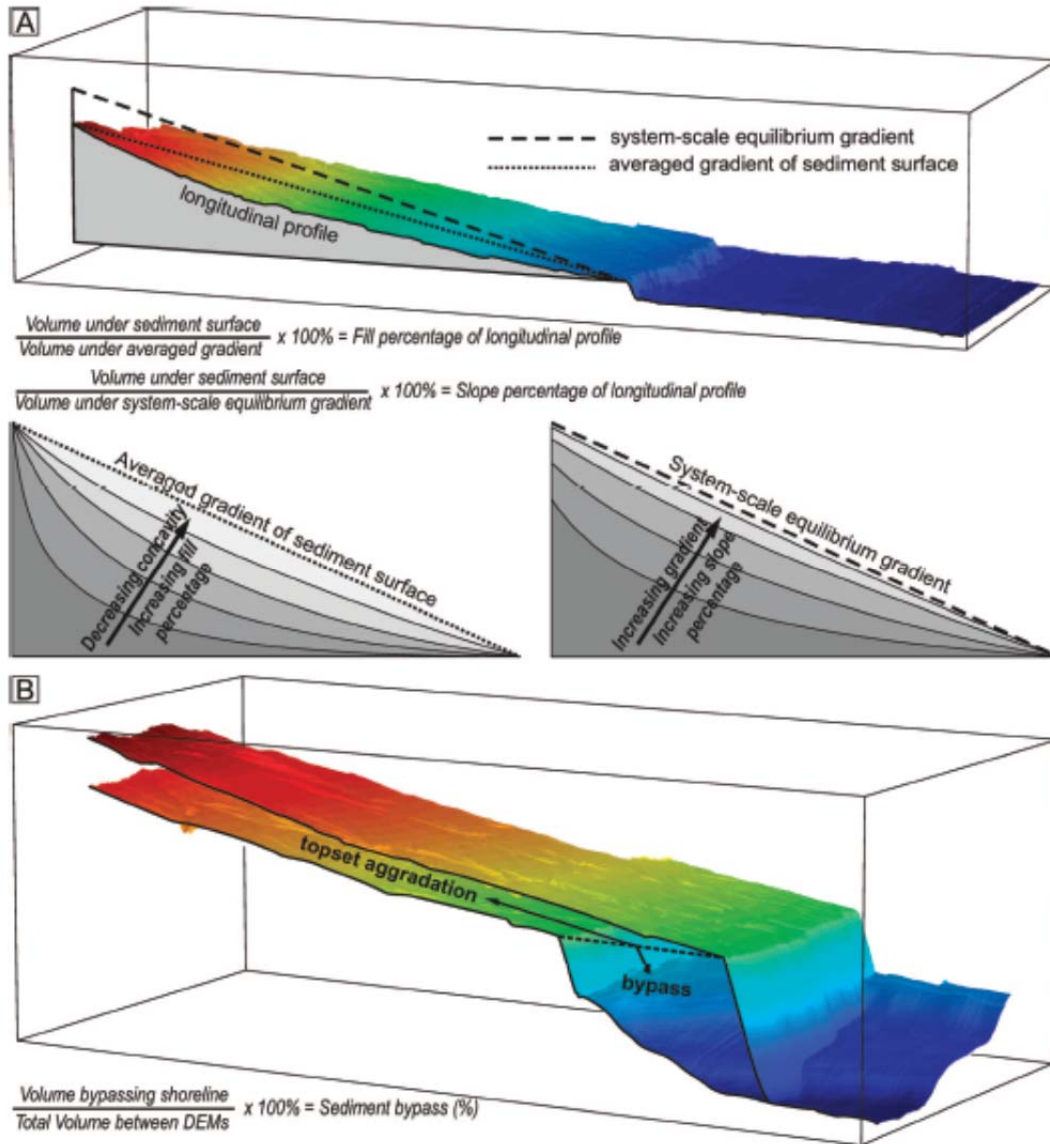
954

955 FIG. 2: (A) Top view of the experiment setup, consisting of two mirror-image models. Sediment and
 956 water are added at the sediment feeder. In the fluvial zone no tectonic movement occurs. In the
 957 basin, 3 zones of distinct water depth are formed. Dimensions (mm) are indicated in regular font,
 958 gradients in italic font. (B) Side view of the experiment, along transect P-P' in (A).



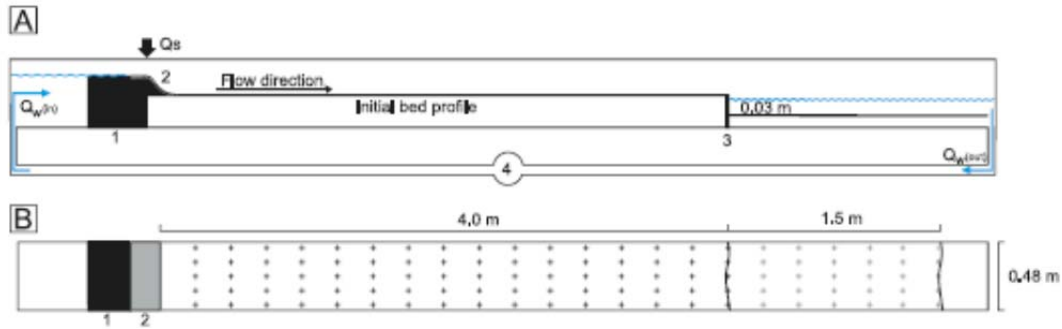
959

960 FIG. 3: Input parameters. The water depth is given for the deep zone of the experimental basin, the
 961 intermediate and shallow zones of the basin have a water depth of $2/3$ and $1/3$ of this value. Note
 962 that in (A) E1_M1, water level and subsidence curves overlay, and in (B) E1_M2, the subsidence and
 963 water depth curves overlay, (C) E2_M1, (D) E2_M2



964

965 FIG. 4: Representation of methods. (A) Fill percentage of the longitudinal profile is calculated as the
 966 volume percentage of a triangle connecting the upstream and downstream ends of the longitudinal
 967 profile (the averaged gradient), and represent a measure of concavity. Increasing fill percentages
 968 thus imply that the system becomes less concave. The slope percentage of the longitudinal profile is
 969 calculated with reference to an estimated system-scale equilibrium gradient and provides an
 970 expression of the longitudinal gradient. See text for discussion of the system-scale equilibrium
 971 gradient. (B) Sediment bypass is calculated as a percentage between the sediment volume
 972 transported past the shoreline of the initial height model, and the total sediment volume between
 973 two successive height models. Note the basin geometry and downdip increase in shelf cliniform
 974 height (model E1_M1).



975

976

977

978

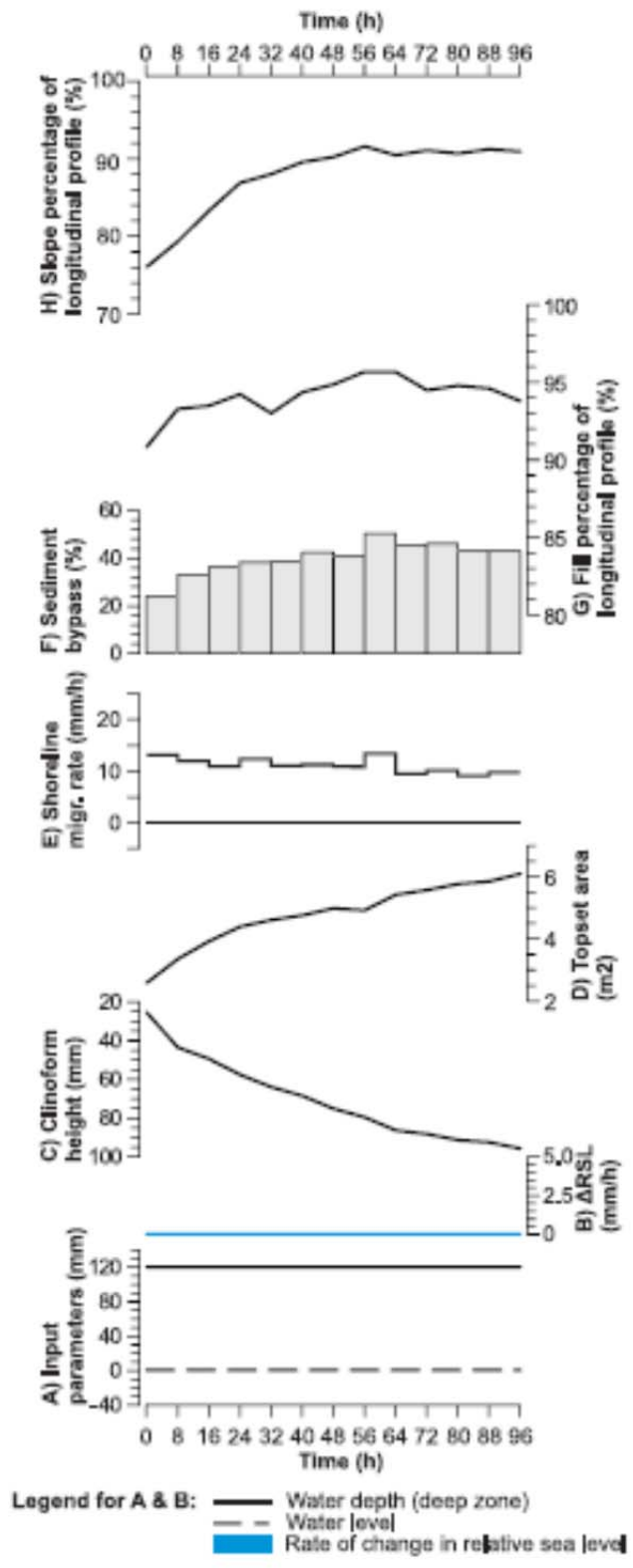
979

980

981

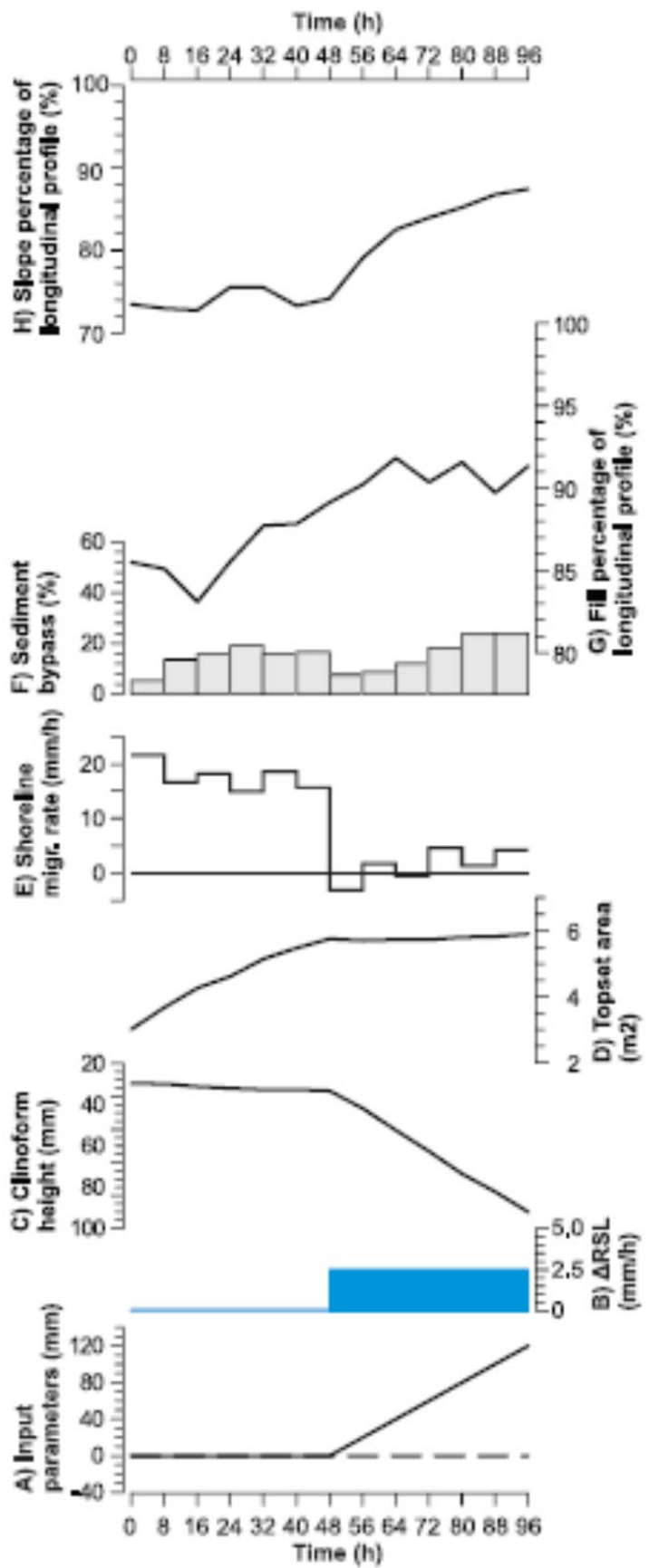
982

FIG. 5: Experiment setup for Scenario 1 and 2. A) Side view of experiment setup. (1) Position of wide upstream weir. (2) Dry sediment is fed from an overhead sediment feeder. Sediment is deposited on a rough cloth that prevents scouring directly downstream of the upper weir. (3) Downstream weir used in Scenario 1. In Scenario 2, this position indicates the initial shoreline. (4) Pump to recirculate water to the upstream weir. B) Top view of experiment setup. Black plus signs indicate locations for height models measurement, grey plus signs indicate additional locations during shoreline progradation.



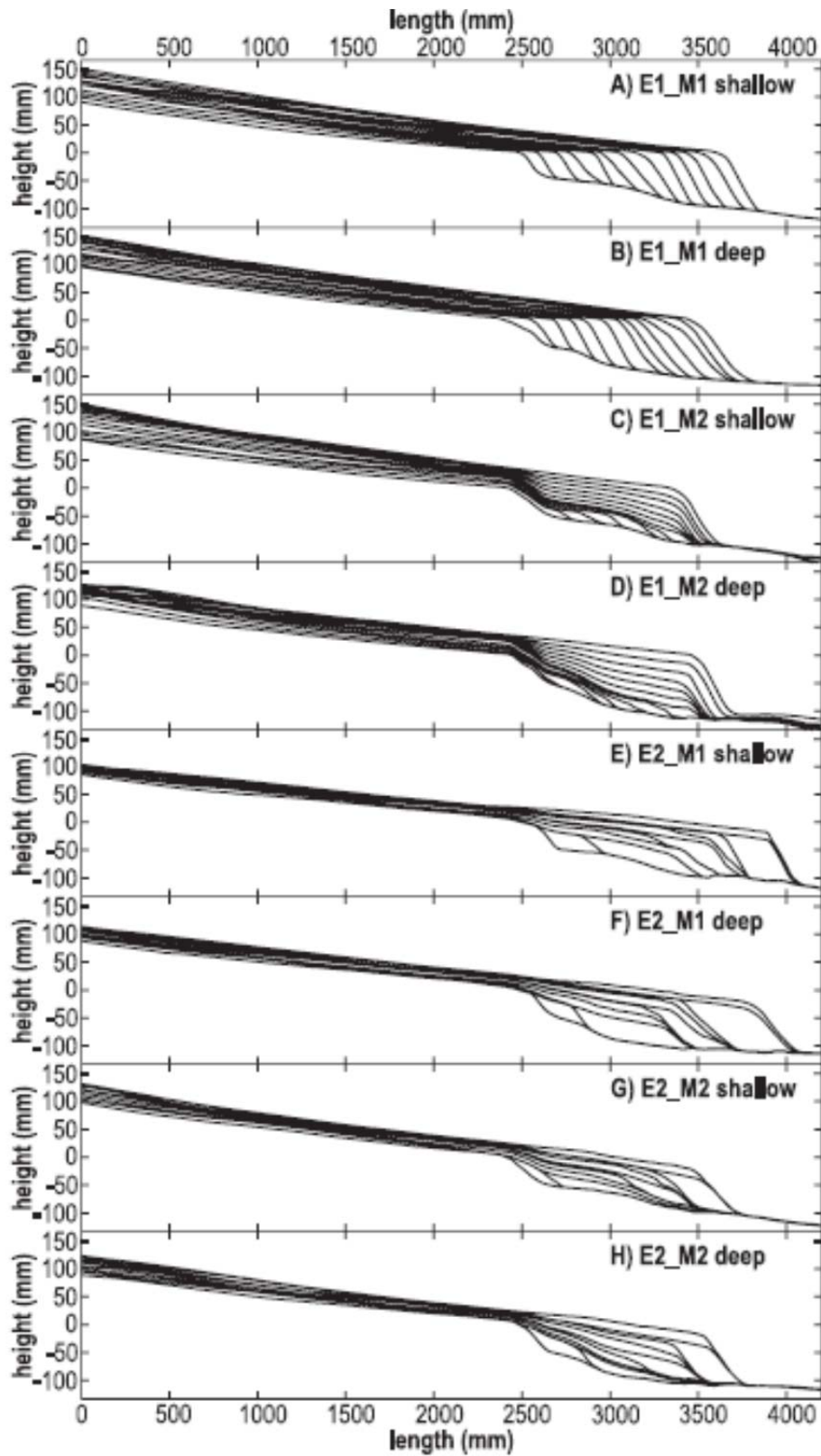
983

984 FIG. 6: Quantitative results for E1_M1. (A) Input parameters for experiments. Note that the water
 985 depth is given for the deep part of the experimental basin, the intermediate and shallow parts of the
 986 basin have a water depth of 2/3 and 1/3 of this value. (B) Rate of change in relative sea level, (C)
 987 Width-averaged water depth (mm), calculated along the strike of the cliniform (D) Topset area, (E)
 988 Progradation rate, calculated between the shoreline of successive height models, (F) Sediment
 989 bypass to beyond the shoreline, see Fig. 4B, (G) Fill percentage of the longitudinal profile, see Fig.
 990 4A. (H) Slope percentage of the longitudinal profile, see Fig. 4A.



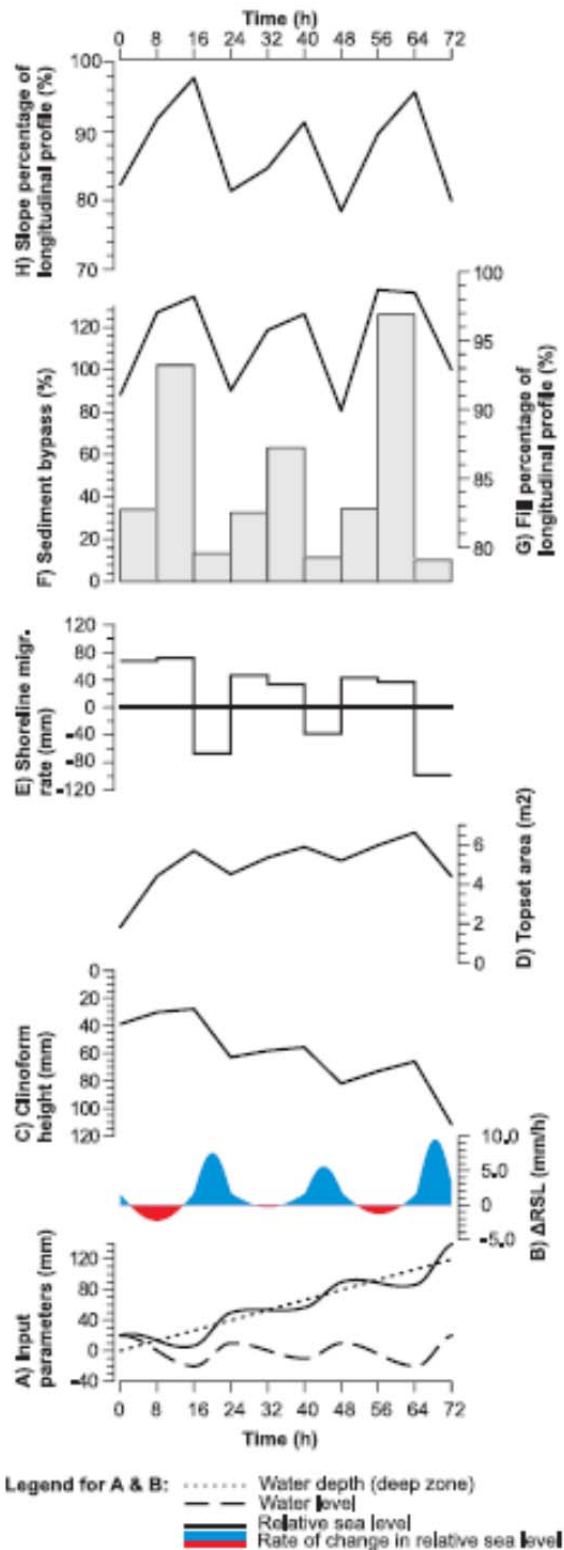
991

992 FIG. 7: Quantitative results for E1_M2. See description at Fig. 6



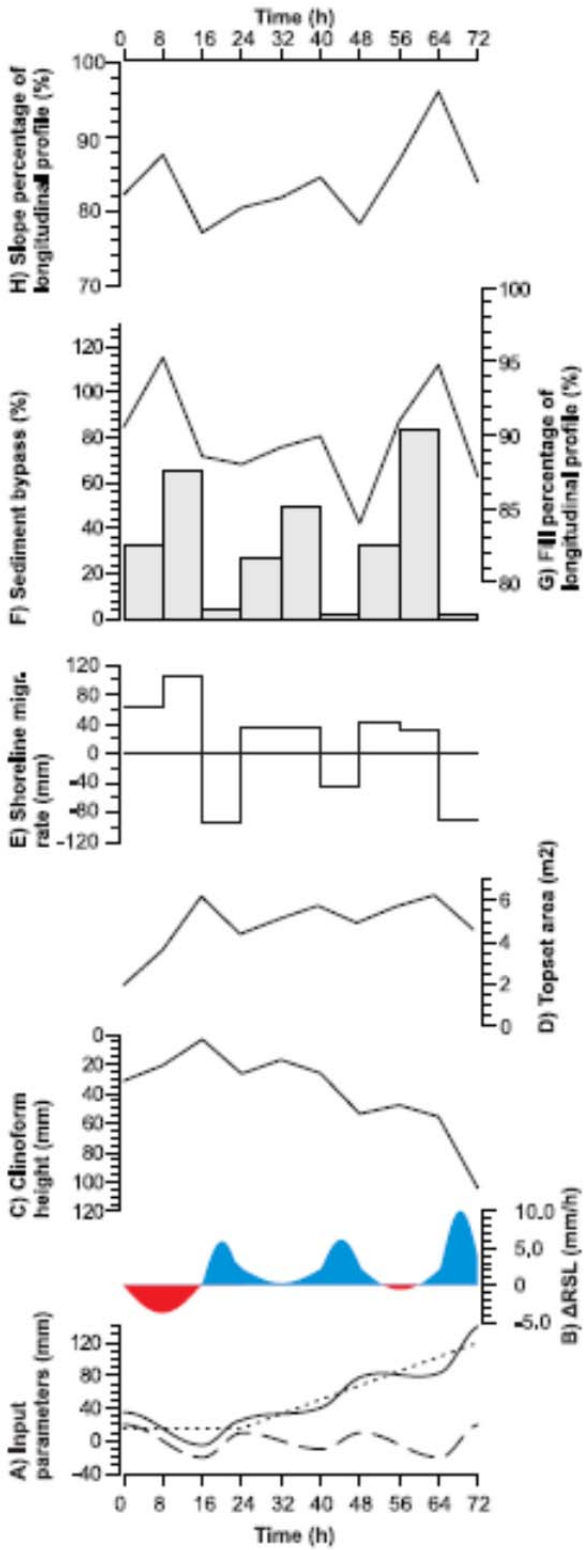
993

994 FIG. 8A-H: Width-averaged transects through the shallow and deep parts of each experiment. Note
 995 that these segments mainly differ in the proximal area of the basin (see Fig. 2A). Each line represents
 996 an increment of 8 h during the experiment.



997

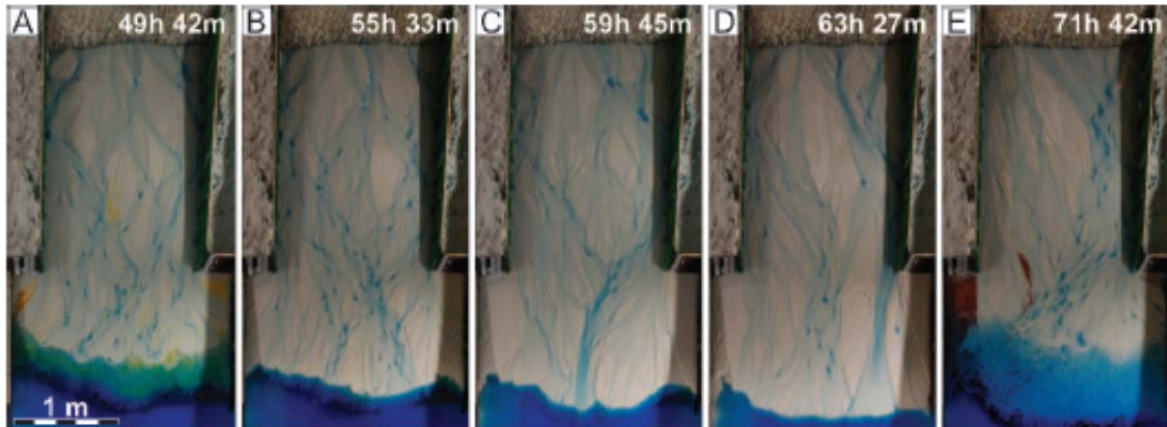
998 FIG. 9: Quantitative results for E2_M1. (A) Input parameters for experiments. Note that the water
 999 depth is given for the deep part of the basin, the intermediate and shallow parts of the basin have a
 1000 water depth of 2/3 and 1/3 of this value. (B) Rate of change in relative sea level, (C) Water depth
 1001 (mm) calculated along the strike of the clinoform (D) Topset area, (E) Shoreline migration rate,
 1002 calculated between the shoreline of successive height models, (F) Sediment bypass, see Fig. 4B, (G)
 1003 Fill percentage of the longitudinal profile, see Fig. 4A. (H) Slope percentage of the longitudinal
 1004 profile, see Fig. 4A.



1005

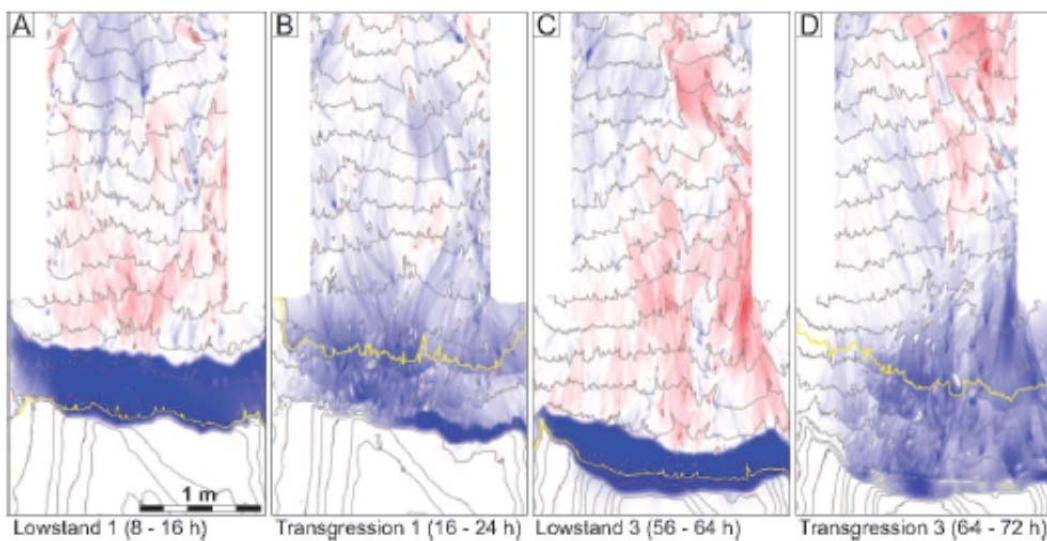
1006 FIG. 10: Quantitative results for E2_M2. See description at Fig. 9

1007



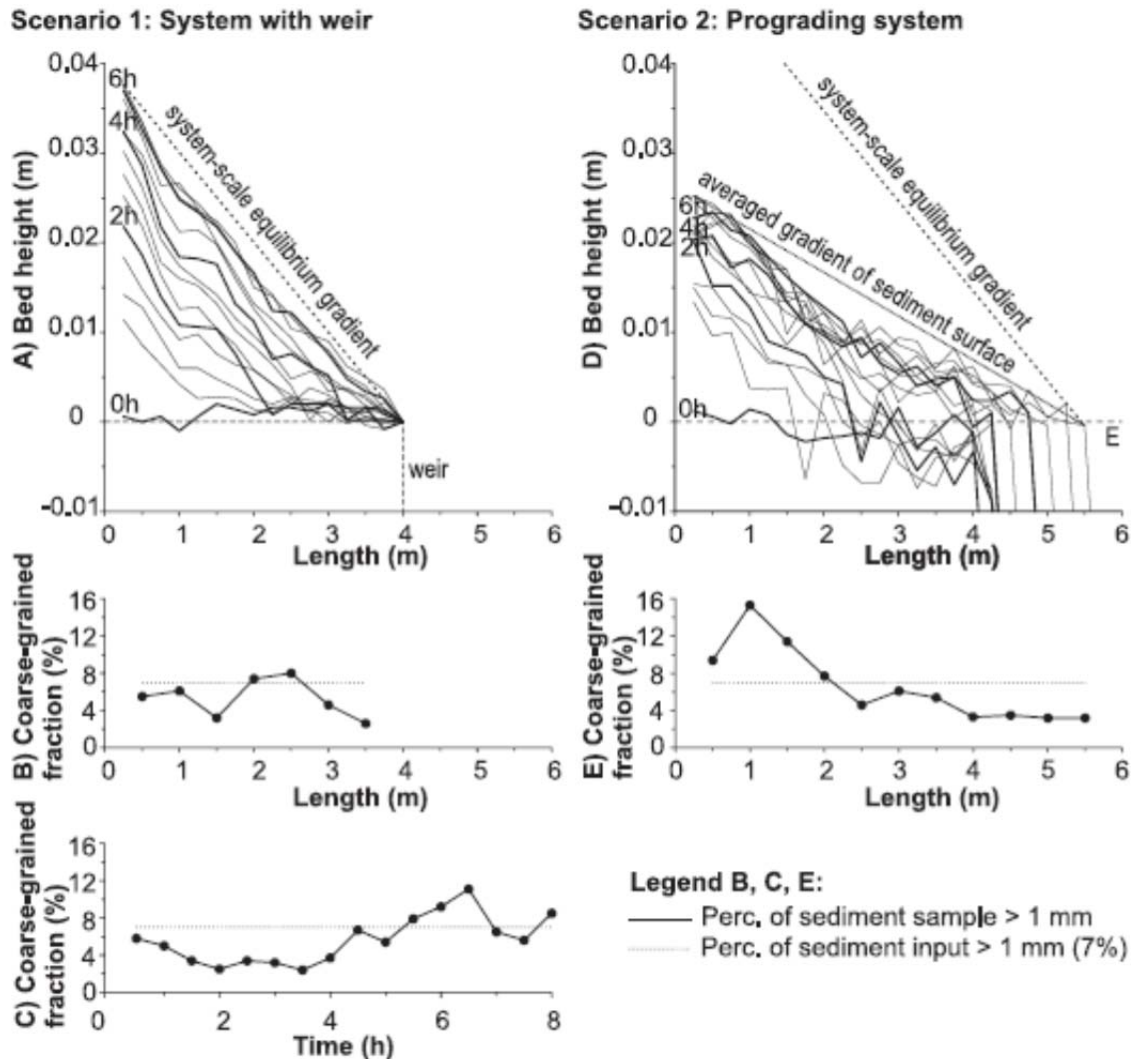
1008

1009 FIG. 11: Photographs of the topset morphology of E2_M1 during sea-level cycle 3. (A) Highstand
1010 Normal Regression, the entire surface area of the topset is frequently wetted. (B) Early Forced
1011 Regression, small interfluvies emerge that are regularly eroded, (C) Incised valley formation during
1012 late Forced Regression initiates at the shoreline of the deep zone of the experimental basin, (D)
1013 Lateral migration of the incised valley mouth after significant progradation of the shoreline widens
1014 the incised valley, (E) Transgression of the distal topset, resulting in a back-stepping coastline.
1015 Continued upstream migration of erosion initiated by the previous sea-level fall increases the
1016 diachroneity of the sequence boundary.



1017

1018 FIG. 12: Erosion-deposition maps for E2_M1. Blue and red indicates respectively deposition and
1019 erosion; increasing color intensity indicates increasing magnitude. Grey contour lines are spaced at
1020 10 mm vertical intervals and indicate topography at the end of the mapped interval. Yellow contour
1021 line represents the shoreline. (A) Lowstand 1 (8 – 16 h), relatively minor erosion and rapid
1022 progradation into the shallow zone of the experimental basin. (B) Transgression 1 (16 – 24 h),
1023 deposition occurs along the entire longitudinal profile. (C) Lowstand 3 (56 – 64 h), erosion is more
1024 severe and has migrated far upstream. Less progradation occurs than in lowstand 1 due to the
1025 significant increase in water depth. (D) Transgression 3 (64 – 72 h), erosion related to the previous
1026 sea-level fall continues updip during the entire sea-level rise while the coastline is characterized by
1027 back-stepping lobes on the lowstand shelf.



1028

1029

1030

1031

1032

1033

1034

1035

1036

1037

1038

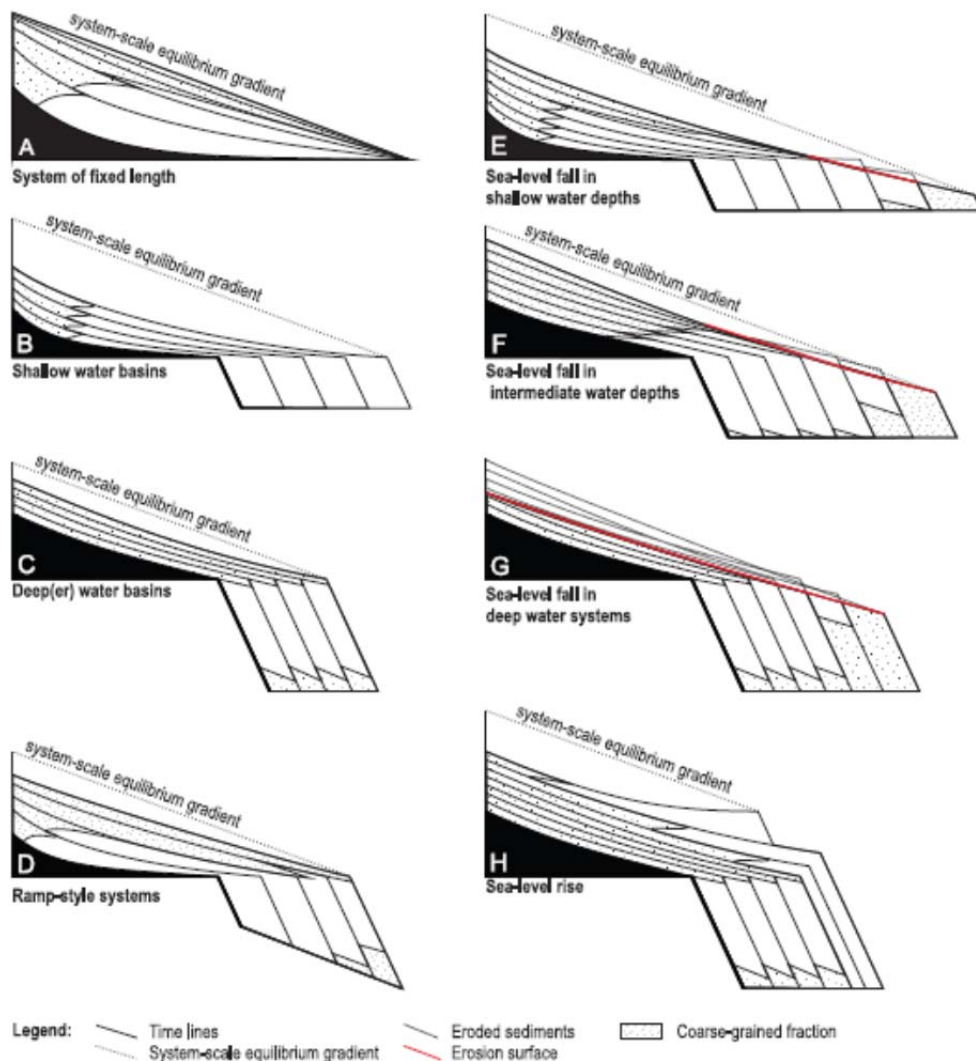
1039

1040

1041

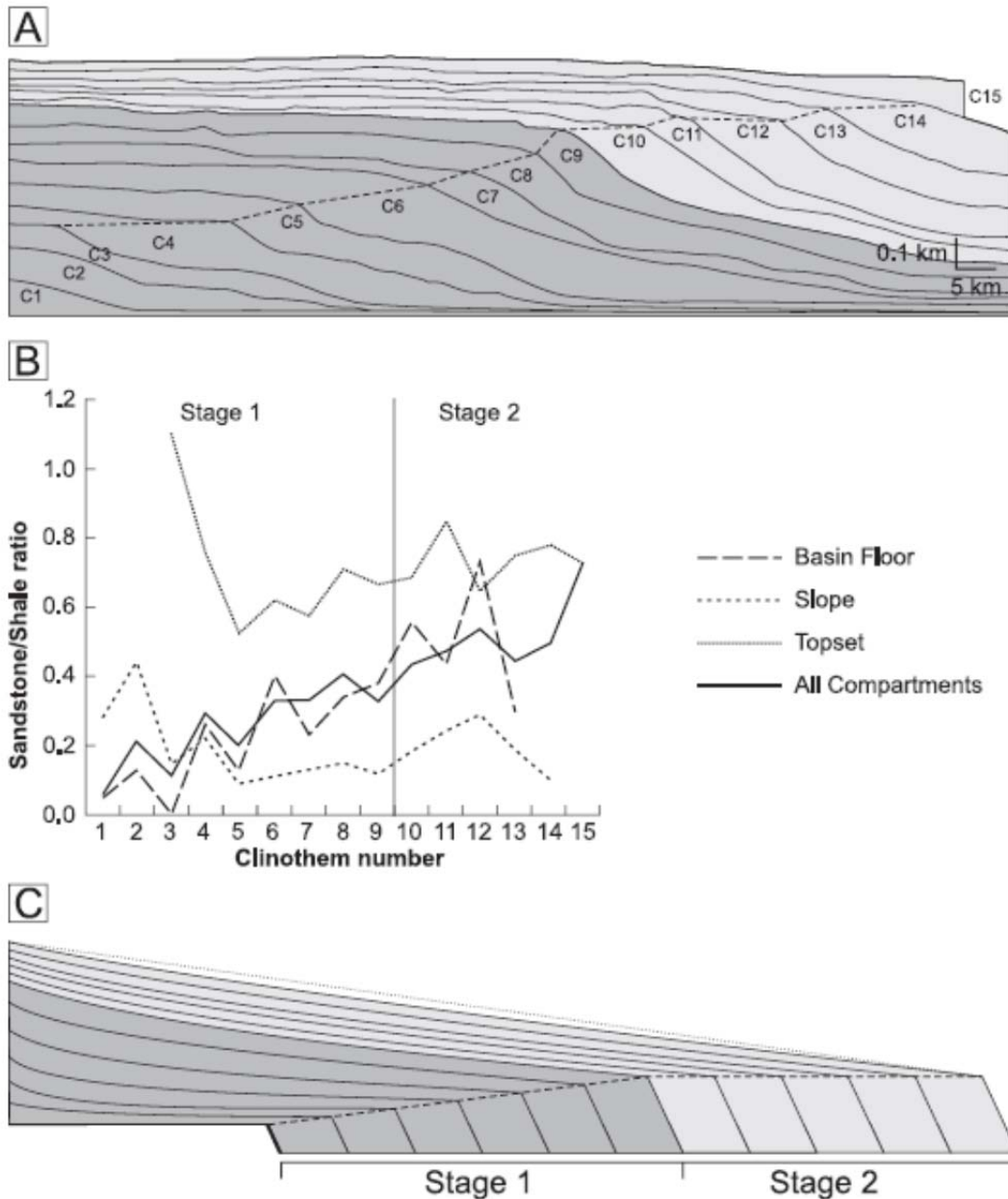
1042

FIG. 13. Longitudinal gradients and downstream fining trends for Scenarios 1 and 2. (A) Longitudinal profiles for Scenario 1 through time. The final profiles overlay each other, implying full sediment bypass along a system-scale equilibrium gradient. The dashed line represents initial bed height and position of weir. (B) Sediment samples collected along the final longitudinal profile of Scenario 1 indicate that the coarse-grained fraction (> 1 mm) is represented along the entire profile without a clear downstream fining trend. (C) Grain-size samples collected below the downstream weir from 0 – 4 h are depleted of coarse-grained fraction, indicating downstream fining. From 4.5 h onwards, input and output of coarse-grained sediment (> 1 mm) are roughly equal indicating that no downstream fining occurs. The peak in coarse-grained sediment (6.5 h) might indicate progradation of a gravel front that accumulated upstream during the earlier stages of the experiment. (D) Longitudinal profiles for Scenario 2. Dashed line indicated by E indicates the water level and initial bed height. Scenario 2 aggrades to a substantially lower gradient than Scenario 1 while upstream conditions are equal. (E) Grain-size samples collected along the final longitudinal profile indicate that the coarse fraction (> 1 mm) is mainly retained in the steep, proximal part of the system (0 – 2 m).



1043

1044 FIG. 14: Influence of water depth on the longitudinal grade of sedimentary systems. Gradients and
 1045 curvature are exaggerated. (A) In a system of fixed length, a system-scale equilibrium profile can
 1046 develop in which the sediment input is equal to the sediment output. (B) In sedimentary systems
 1047 prograding into shallow water basins, high progradation rates lead to strongly concave, low gradient
 1048 longitudinal profiles in which coarse sediment is largely retained upstream. Large sediment volumes
 1049 are sequestered in the relatively high accommodation fluvial system. (C) The longitudinal profile of
 1050 fluvio-deltaic systems prograding into deeper water can approach system-scale equilibrium more
 1051 closely because of low progradation rates, resulting in high sediment transport rates to the coastline
 1052 and limited downstream fining. (D) Fluvio-deltaic systems prograding into deepening water in ramp-
 1053 style settings will approach system-scale equilibrium more closely, gradually increasing sediment
 1054 bypass to the shoreline and decreasing in downstream fining. (E) Relative sea-level fall in shallow
 1055 water systems or on a shelf. Rapid progradation will impede erosion but sea-level fall is still likely to
 1056 increase the gradient and decrease the concavity of the longitudinal profile, increasing the efficiency
 1057 of sediment transport along the longitudinal profile and reducing downstream fining. (F) In
 1058 moderate water depths, for example shelf clinofolds of small height, relative sea-level fall can lead
 1059 to significant erosion and high sediment bypass beyond the shoreline during late falling stage and
 1060 lowstand. (G) The likelihood of valley incision depends on the rate and amplitude of sea-level fall but
 1061 also increases with increasing water depth. Valley incision can result a lowering the system-scale
 1062 equilibrium gradient within the incised valley. (H) Sea-level rise results in an increased concavity of
 1063 the longitudinal profile and strong downstream fining, resulting in fine-grained highstand systems
 1064 aggrading on the lowstand shelf deposits.



1065
 1066 FIG. 15: (A) Clinothem succession of the Maastrichtian Lance - Fox Hills – Lewis Shelf Margin,
 1067 Southern Wyoming. Note that the aggradational succession in Stage 1 (C1-C9) represents a relative
 1068 sea-level rise, and Stage 2 (C10-C15) a progradational succession during relative sea-level still stand.
 1069 Simplified from Carvajal and Steel (2006). (B) Sand/shale ratios for individual clinothems, modified
 1070 from Carvajal (2007). (C) Alternative interpretation of sediment volume and grain size trends, with
 1071 strongly exaggerated gradients in which the differences in sediment supply and grain size are
 1072 attributed to the response of the longitudinal profiles to changes in water depth and basin
 1073 development.

1074